Gonçalo Filipe Fernandes Narciso

Licenciado em Ciências de Engenharia de Micro e Nanotecnologias

In-Depth X-Ray Photoelectron Spectroscopy of Resistive Switching Devices

Dissertação para obtenção do Grau de Mestre em
Engenharia de Micro e Nanotecnologias

Orientador: Doutor Jonas Deuermeier, Investigador Doutorado, Faculdade de Ciência e Tecnologias da Universidade Nova de Lisboa

Co-orientador: Doutora Asal Kiazadeh, Investigadora Doutorada, Faculdade de Ciência e Tecnologias da Universidade Nova de Lisboa

Júri:

Presidente:	Prof. Dr. Rodrigo Fernão Paiva Martins
Arguente:	Prof. Dr. Joana Dória Vaz Pinto
Vogal:	Dr. Jonas Deuermeier

Setembro de 2019

FACULDADE DE CIÊNCIAS E TECNOLOGIA
UNIVERSIDADE NOVA DE LISBOA

In-depth X-Ray Photoelectron Spectroscopy of Resistive Switching Devices

Acknowledgements

In first place, I'd like to thank Professor Rodrigo Martins and Professor Elvira Fortunato, for their most valuable work and dedication in development of the Micro and Nanotechnology course and of the Centre of Investigation in Materials (CENIMAT) and from Department of Science and Materials (DCM) giving us students a wide range of opportunities to make science.

I'd also like to thank the Faculty of Science and Technology of Nova University of Lisbon for providing excellent college conditions, giving to the students the best preparation they need before entering in the labour world.

Thirdly, I want to thank my supervisor Doctor Jonas Deuermeier for always be available for helping me on all occasions and to clarify all of my numerous XPS doubts. Most importantly, thank you for calling my attention and to correcting all my errors in a constructive manner that allowed me to evolve as a researcher. All of your tips gave me the ability to understand much better how to properly do science work.

Also, a big thanks to my other supervisor Doctor Asal Kiazadeh for all of the electrical pieces of advice in the memory's electroforming, without them maybe I would not have a single resistive switched device to properly analyse. Also, would like to thank the remaining members that made part of the Neuroxide team: Ana Rovisco, Emanuel Carlos, Nuno Casa Branca, Ricardo Nogueira, João Carlos, Joana Cristina, Jorge Martins and Maria Pereira.

To the last two elements of the group mentioned, I would like to give a special acknowledgement. First, to Maria that had to tolerate all my beginner's slow work in the cleanroom that consumed a lot, but really a lot of her time. Thank you for helping not only, in the cleanroom, electrical characterization, correcting my thesis and whenever I needed. But most importantly thank you for all the things that you did for me, that help me a lot in a professional and personal way. Also, thank you Jorge, for helping me with the simulation work of the parameters of the rectifier behaviour in ITO/GIO/Au device.

Thank you to Cátia and Inês Martins for helping with the sputtering of GIO. And to Sara Silvestre for the laser cutting of my glass substrate and masks.

Thanks to Hasan Arif Yetkin from HZB Berlin institute, for sharing ideas and details from your work that made possible the fabrication of the ITO/GIO/Au resistive switching device studied.

I also want to thank my college colleagues throughout my course, especially Pedro Centeno and Xavier Mascarenhas that made this course much easier with all of the fun that we had and surely, we will have in the future. I will take you both for the rest of my life. My friends from LaFamilia, you are my second family, you are my brother and sisters and your support made me have the strength to finish a master thesis.

Also, thank you to the person that made me grow a lot as a person in 3 and a half years, Mia. You really were important, I could write another and a longer thesis about it.

Lastly, but without a doubt the most important thank you goes for my parents and my brother. I am so grateful for having always your support. I am who I am because of you, you gave me everything, all the tools that I needed you provided. Thank you, this work is dedicated to you, my wonderful family.

Abstract

This work has explored the possibility of using x-ray photoelectron spectroscopy (XPS), for studying the chemical properties (i.e. atomic ratios and oxidation states) of several metal-insulator-metal (MIM) structures. This thesis aims to better understand the operation mechanism that imposes a reversible change in the resistance state of the studied devices. Three different configurations (ITO/ZTO*/Pt, Pt/ZTO/Ti-Au, ITO/GIO*/Au) were fabricated following a physical vapour deposition methodology and patterned using shadow masks, specifically designed for this purpose. An electrical characterization was performed first, to evaluate the uniformity between the devices through the study of their pristine state and second, to change the resistance state, applying a high voltage signal, followed by an in-depth XPS analysis.

The XPS argon cluster depth profiling of the produced MIM structures showed that the resistive switching mechanism of the Pt/ZTO/Ti-Au device was not ionic, since no change of cation ratios and oxidation states were observed throughout the depth of the device, comparing pristine state and the low resistive state (LRS). The ITO/GIO/Au device exhibited area-dependent electroforming, which led to an irreversible change in the forward direction. Remarkably, the diode was free of any hysteresis after electroforming. The XPS depth profile revealed an increased indium concentration within the bulk region near the ITO after electroforming, compared to the pristine state of the device. Hence, despite being irreversible, the resistance change of the device is clearly related to an ionic mechanism.

*ZTO: zinc-tin oxide; GIO: gallium-indium oxide

Keywords: X-rap photoelectron spectroscopy, resistive switching, depth profiling, diode.

Resumo

Este trabalho explorou a possibilidade de usar a espectroscopia de fotoeletrões de raios X (XPS), para estudar as propriedades químicas (por exemplo, relações atómicas e estados de oxidação) de várias estruturas metal-isolante-metal (MIM). Esta tese visa compreender melhor o mecanismo de operação que impõe uma mudança reversível no estado de resistência dos dispositivos estudados. Três configurações diferentes (ITO / ZTO * / Pt, Pt / ZTO / Ti-Au, ITO / GIO * / Au) foram fabricadas seguindo uma metodologia de deposição de vapor físico e padronizadas usando máscaras de sombra, projetadas especificamente para essa finalidade. Uma caracterização elétrica foi primeiro realizada para avaliar a uniformidade entre os dispositivos através do estudo do seu estado primitivo e em segundo, para alterar o estado de resistência, aplicando um sinal de alta tensão, seguido de uma análise XPS em profundidade.

O perfil de profundidade do cluster de argón XPS realizado nas estruturas MIM produzidas mostrou que o mecanismo de comutação resistiva do dispositivo Pt / ZTO / Ti-Au não era iónico, uma vez que não foram observadas alterações nas razões de catiões e estados de oxidação em toda a profundidade do dispositivo, comparando o estado primitivo e o estado de baixa resistividade (LRS). O dispositivo ITO / GIO / Au exibiu eletroformação dependente da área, o que levou a uma mudança irreversível na direção direta. Notavelmente, o diodo estava livre de qualquer histerese após a eletroformação. O perfil de profundidade do XPS revelou um aumento da concentração de índio na região bulk próxima ao ITO após a eletroformação, em comparação com o estado primitivo do dispositivo. Portanto, apesar de irreversível, a mudança de resistência do dispositivo está claramente relacionada a um mecanismo iónico.

* ZTO: óxido de zinco-estanho; GIO: óxido de gálio-índio

Palavras-chave: espectroscopia de fotoeletrões raios-X, comutação resistiva, perfil de profundidade, diodo.

List of Abbreviations

AE – active electrode
AFM - atomic force microscopy
BE - bottom electrode
CC - current compliance
CMOS - complementary metal-oxide-semiconductor
HAXPES - hard X-ray photoelectron spectroscopy
HRS - high resistive state
HSA - hemispherical analyser
GIO - gallium-indium-oxide
LRS - low resistive state
MIM - metal-insulator-metal
NVM - non-volatile memory
RRAM - resistive random-access memory
RS- resistive switching
RT - room temperature
TE - top electrode
XPEEM - X-ray photoemission electron microscopy
XPS - X-ray photoelectron spectroscopy
ZTO - zinc-tin-oxide

Table of contents

List of Figures

List of Tables

Motivation and objectives

The modern and conventional memory technology based on the complementary metal-oxide-semiconductor (CMOS), such as NAND Flash, DRAM, and SRAM, for the past decade, had their performance increased by the miniaturization of the integrated transistors and capacitors. This method raises problems of cost-efficiency for the industry, because of the more challenging and expensive integration of the transistors in the architecture of the memory during the fabrication. The miniaturization of these memories is also getting to a physical limit, so another technology is required that gives an industrial solution to this problem. [1]

The technological solution must achieve a high-density storage of information at a low-cost. These requirements can be potentially fulfilled by the resistive random-access memory (RRAM) technology, this technology allows the switch from the charge storage realized by a capacitor of the CMOS technology, to a resistance change of the materials that will store the information. The resistance change is commonly known as resistive switching and can occur as at least two device states, a high resistive state (HRS) when the cell is OFF and a low resistive state (LRS) when the cell is ON. [2] Also, a very interesting area explored with the resistive switching (RS) mechanism is the emulation of synapses for artificial neural networks. Interfacial resistive switching has to happen in these devices in an analog way to resemble the synaptic behaviour.

The resistive switching is caused by physical or chemical nanoscale switching mechanisms that change the resistance of the material that is between two terminals when a voltage is applied. The common way to classify the type of resistive switching mechanism that occurs in the structure of a memory is studying the I-V (current-voltage) characteristics and hysteretic behaviour. The physical and chemical mechanisms responsible for the resistive switching are well categorized but are not totally understood. [1]

The focus of this thesis falls on the studying and the better understanding of the resistive switching mechanisms, by complementing the I-V characteristics behaviour with X-ray photoelectron spectroscopy (XPS) analysis. The purpose of using the XPS technique is to study the chemical processes, like reduction and oxidation of the atomic elements near the interfaces with the terminals (top and bottom electrodes) when a previously applied voltage modified the resistive state of the device. An in-operando approach was tested inside the main-chamber of the XPS to modify the state of the device. After that, the elemental concentrations and oxidation states were studied by argon cluster depth profiling of devices in different resistance states

Memory and synaptic electrical properties were shortly analysed, being only performed some initial tests. This research centred on the XPS potential to study interfacial-type switching occurring in the devices.

In this study, three devices were fabricated having a metal-insulator-metal (MIM) structure, and layers were deposited by physical vapour deposition methods: the oxides GIO (gallium-indium oxide), ZTO (zinc-tin oxide) and ITO (indium-tin oxide) were deposited via-sputtering. The metals were deposited by electron beam evaporation, except for molybdenum, which was also deposited by sputtering. All of these devices and layers will be patterned with shadow masks designed to fit to the sample holder of the XPS instrument and to allow the realization of the in-operando approach inside the XPS main-chamber. Electrical characterization of devices will be realized before all XPS

analysis, studying the pristine rectification ratios and hysteretic behaviour of the I-V characteristic. The I-V tests will give an initially idea of which switching mechanism is occurring in each device, and later be discussed in concordance to the XPS analysis.

1 Introduction

1.1 Resistive Switching

Resistive switching (RS) is a physical phenomenon that occurs in an electrical insulator material (oxide materials are the most intensively studied) when an application of an external electric field consequently causes reversible changes in the metastable resistance state. This means that, for example, a film with insulator properties between two metal electrodes (MIM structure) shows a significant resistance drop when the applied voltage is further increased. At the same time, the conductance in the device increases several orders of magnitude reaching a new resistance state called low resistive state (LRS).[3] What distinguishes the resistive switching devices is that the induced state in the previous example can be reversible back to a high resistive state (HRS), and even be switched between both states several cycles by controlling the voltage applied in the electrodes. Another very important characteristic of the resistive switching devices is that they can exhibit non-volatile memory properties.[4]

Two types of RS behaviours can be distinguished from the I-V characteristics: unipolar and bipolar switching. Unipolar RS means that the resistance switching hinge on the intensity of the electric field. It is necessary to apply high voltage in the device in order to reach an LRS or ON state (set process). The reverse process is called reset when the device goes from ON state to OFF state or HRS. On the other hand, bipolar switching occurs when the set process occurs in one voltage polarity and the reset happens in the opposite voltage polarity.[5]

The resistive switching is electrically induced in almost every device with this property, but the physical mechanisms that are responsible for the reversible changes in the resistance state are quite different. [6] Figure 1.1 organizes the main and well-known switching mechanisms and the effect that each one of them has on a device.

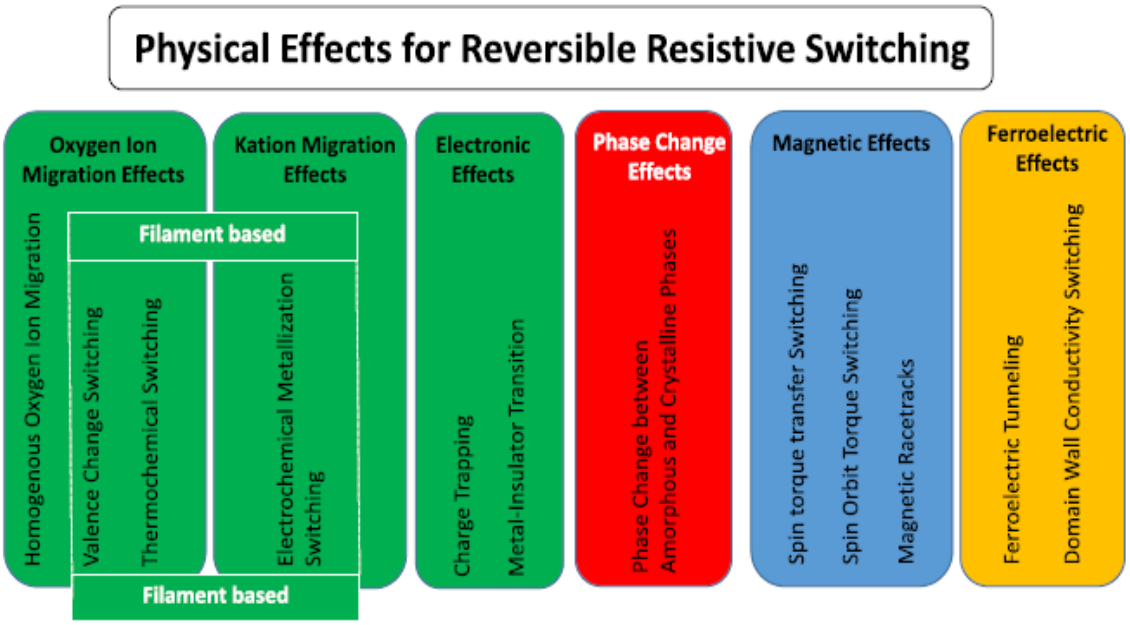

Figure 1.1 General overview of the main physical mechanisms of resistive switching and the effects that each one of them has over the integrated device. [1]

Several categories of resistive switching effects displayed in Figure 1.1 distinctively classify the major non-volatile MIM structures. The RS filament-based types (1D-RS) are one of the most promising devices in non-volatile RRAM memories but have drawbacks to this technology like the unevenness in electrical measurement in the devices. Another characteristic of the filamentary switching is the abrupt set and reset processes. This problem is a handicap to artificial neural networks studies that intend to emulate the synaptic behaviour using analogue switching. The interfacial type switching (2D-RS) is required to occur in a gradual (and not abrupt) way, the set and reset processes. [7], [8]

Figure 1.2 illustrates the differences between the resistive switching processes in the filamentary conducting path (Figure 1.2 (a)) and the interfacial conducting method (Figure 1.2 (b)).

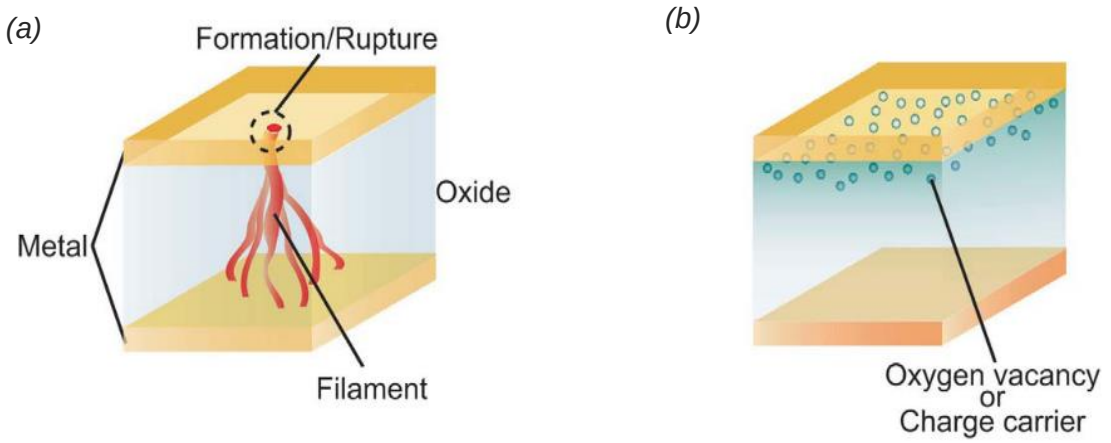

Figure 1.2 Resistivity switching models of (a) the filament-type switching and (b) the interfacial type switching. [9]

This interface type of RS described in Figure 1.2 takes place at the interface between the active electrode (AE) and the oxide layer. This type of RS shows bipolar I-V characteristics behaviour and is area-dependent (the bulk 3D-RS shows this area dependency too). [9] This area-dependent RS can be explained by a homogeneous change in the tunnel barrier height induced by homogeneous migration of defects (oxygen vacancies are the most common type of defects in oxides) or ions through the switching insulator layer. [8], [10] Several mechanisms can be associated with these homogeneous migrations. Such as the thermionic (Schottky) that happens when thermally-activated electrons are injected over the energy barrier into the conduction band of the oxide. [7]

However, electronic effects can also be responsible for this type of RS. The charge trapping mechanism is an example of these electronic mechanisms, that can change either 2D properties between the metal electrodes and the insulator or modify the band structure in the 3D bulk insulator. Both in 2D-RS and 3D-RS, AE can form a Schottky junction with the insulator layer and show rectifying hysteresis behaviour in I-V characteristics in this interface. [9] This electrical behaviour represents the phenomenon of electronic charges from the metal electrode being injected and fill all the traps in the insulator layer. When this occurs, I-V characteristics show an exponential increase of the current correlated to resistance change of the device to LRS. [11]

1.2 X-Ray Photoelectron Spectroscopy (XPS)

X-ray photoelectron spectroscopy is a photoemission technique, that relies on the photoelectric effect. [12] Photons with well-defined energy are focused on a sample's surface and this excitation causes electron emission. The emission will happen if the photons have higher energy than the binding energy of the excited electrons plus the materials work function. Counting the photoelectron with respect to their kinetic energy results in an energy spectrum, that shows specific characteristic peaks of the electronic structure when the core level electrons are emitted from the atoms of the first 6-9 nm of the sample. [13], [14]

The XPS instrument, fundamentally, includes an x-ray source, an ultra-high vacuum chamber, an electrostatic transfer lens system, a hemispherical analyser (HSA), an x-ray detector, a charge neutraliser and a stage for the sample be analysed. The instrument configuration is shown in Figure 2.3.

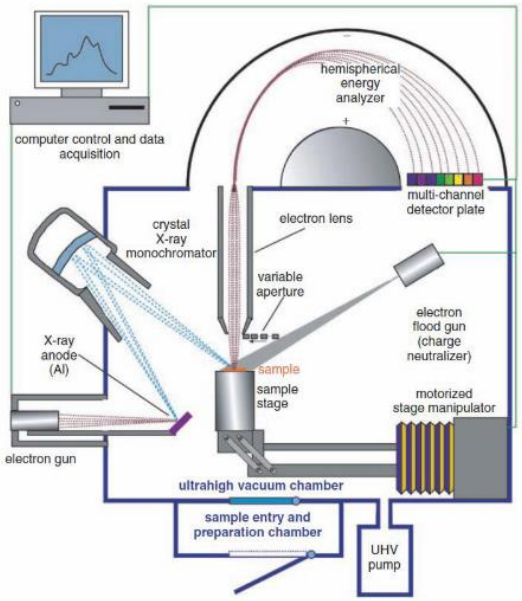

Figure 1.3 X-ray photoelectron spectroscopy instrumentation's schematic. [11]

Typically, the x-rays source is composed of an electron gun that generates a high-energy electron beam (around 5-20 keV) onto anodes of Mg or Al, for example, and generates photons of known energy like 1253.6 eV and 1486.6 with energy widths of 0.7 and 0.85 eV, respectively. Coupling x-ray monochromators to the anodes will reduce the energy width and will give a more precise energy resolution. [14]

The main chamber of the XPS is in ultra-high vacuum with pressures below 10^{-11} bar. Since scattering with gas molecules reduces the inelastic mean free path of the photoelectron, this ultra-high vacuum is necessary so that the electron can reach the detector without an energy loss.

The HSA and the electrostatic transfer lens work together to assure that only electrons with a determined kinetic energy arrive at the detector. This is fundamental to realize high-resolution spectra with a specific interval of energy defined by the user within the limits of quantum mechanics. The electrons, when in the transfer lens system have to pass through a specific aperture of the lenses and are focused into the entrance slit of the HSA. The analyser has the function of only allowing the specified range of energy to reach the detector, retarding any electron that enters the analyser with a higher velocity

than the desired one. [15] A scan of the retardation voltage results in the scan over the whole kinetic energy range.

When an insulating sample is put on the stage of the main chamber, electric charges can accumulate at the surface of the sample when the photoemission of electrons is occurring. To prevent this phenom that can cause a shift in the spectrum of the sample, a charge compensation mechanism is used, based on a low-energy electron flood gun.

1.2.1 XPS analysis

As previously said above, the binding energy is normally calculated and shown in the spectra of the XPS analysis. The binding energy can be calculated after analysing the kinetic energy of the ejected photoelectron:

$$BE = h\nu - KE - \phi \quad (1.1)$$

where the binding energy is BE, KE is the kinetic energy of the emitted electron, *hv* is the photon energy and ϕ the work function of the spectrometer.[11]

Figure 1.4 (a) portrays the photoelectric effect when a photon interacts with an electron in an atomic orbital. Figure 1.4 (b) displays a general example of an XPS spectrum with the intensity of electrons (counts per second) as a function of binding energy (eV).

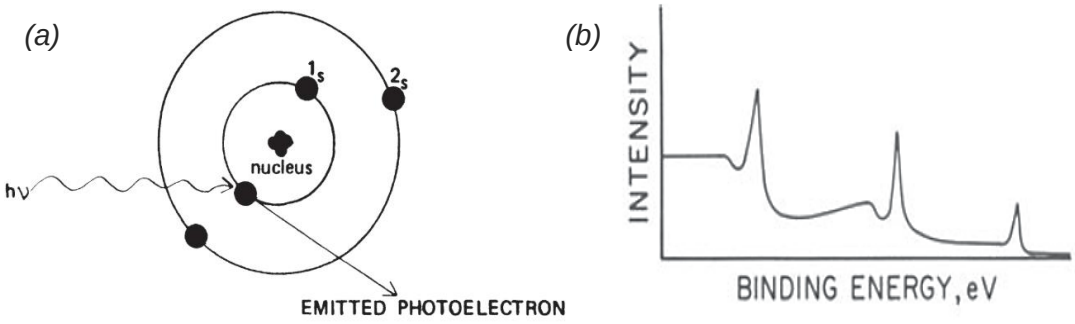

Figure 1.4 (a) Photoelectric principle (b) Example of a typical XPS spectra. Adapted from reference [15]

XPS is the most used technique when analyzing the chemical constitution of a sample's surface, as a result of the valuable information of peak intensities and binding energy position of the same peaks. [14] When starting analyzing the peaks in the spectrum, the user has to realize a background subtraction based on two physical approaches, the Shirley [16] and the Tougaard [17] methods. Shortly explained, these backgrounds methods take into account the inelastic losses of the primary photoelectrons. Shirley said that his background method is proportional to the integral of the number photoelectrons excited. [16] Tougaard showed that different energy losses occur in different photon energies, for different elements in the sample, and for that reason he proposed a function that derives the loss inelastic background in a distribution curve. [17]

Another important step is realizing a curve fitting to identify the different chemical bonds in a specific element. There are symmetric line-shapes that can be traced, by the convolution of Lorentzian and Gaussian curves. Metal peaks usually use asymmetric lines that are product of modifying the parameters like gaussian component's width and spread the tail of the Lorentzian component.[18] Generally, oxidation leads to a higher binding energy, whereas reduction leads to a lower binding energy.[14]

XPS allows to analyse only the first few nanometres of the surface of the sample, since characteristic peaks arise only from electrons detected without energy loss by

inelastic scattering, despite the ionization occurring also in greater depths. It is possible to study the chemical properties in the whole depth of the sample, recurring a technique referred to as depth profile analysis. This technique is based on a controlled erosion of a sample's surface, using an ion sputtering gun composed by, normally, a beam of 500 atoms of Ar^+ ion clusters. The analysis obeys a regular step sequence defined by the researcher, where the bottom of each etched crater formed after each sputtering is analysed after focusing again the x-rays. This gives the opportunity to know the chemical properties in all depth and of the layers composed in the sample. [19], [11]

In many researches, the XPS is utilized due to its ability to provide the data needed to determine the atomic ratios and relative concentrations, between the elements present in a sample, and allows the study of the chemical stoichiometry. The atomic ratio of any constituent in a sample can be calculated using the following general expression:

$$A_x = \frac{I_x/S_x}{(\Sigma I_x/S_x)}, \quad (1.2)$$

where A_x is the atomic concentration, I_x is the photoelectrons counts per second in a specific peak and S_x is the atomic sensitivity factor. This sensitivity factor values have to be tabled for each element and have to be adjusted for each XPS instrument, because of the corrected transmission function of each spectrometer detector.[19]

1.3 Up-to-date research of Resistive Switching and XPS

Nowadays, it is still very difficult to understand the resistance switching phenomena when talking about the chemical processes that influence the stoichiometric changes in elements of the sample. [20]

There are a few studies in the literature that study this resistive properties in RRAM memories, with similar techniques to XPS, like hard x-ray photoelectron spectroscopy (HAXPES) and X-ray photoemission electron microscopy (XPEEM). [13], [18], [21], [22], [23] Other technique that is widely used to characterize the physical mechanisms of the resistive switching, is the atomic force microscopy (AFM). This technique has a unique capability to realizing highly localized in situ and ex-situ studies, and these studies had a significant scientific contribution to the field of RS in the last few years. [24] However, definite chemical contrast is not possible be obtained by AFM.

This thesis aims to study in more depth the chemical properties in the resistive switching, analysing the chemical states and compositions of the metal and oxide components in the elements of the layers and interfaces of several MIM structures. An innovative in-operando XPS approach is discussed, which allows the resistive switching to happen inside the main chamber in ultra-high vacuum. Since usually large-scale facilities (synchrotron) are needed for HAXPES and XPEEM, for example, it is innovative to investigate in-operando and in-depth analysis possibilities using a state-of-the-art lab-based spectrometer.

2 Materials and Methods

2.1 Shadow Masks Fabrication

The devices were fabricated with the purpose of being electrically characterized inside XPS.

Firstly, two shadow masks were designed in this thesis, to work specifically with the XPS holder. The masks are represented in Figure 2.1 and were designed in Adobe Illustrator, to fit in a homemade mask support that allows the fabrication of four 2.5 × 2.5 cm^2 samples. In Figure 2.1 (a) it is presented the design and of the back electrode (BE) of each device. It has a rectangle with 2.1 cm width and 0.5 cm height, where the back contact of the holder will be connected. Also, it has 3 lines with 0.1 cm where the overlap with the other layers will occur. The design presented Figure 2.1 (b) was also utilized as the shadow mask, but this time to fabricate the top electrode (TE). This last mask allows the contact with a needle connected to the top contact of the holder, for that reason is used 0.1 cm width lines.

Lastly, both masks were sent to a professional for fabrication in an aluminium plate.

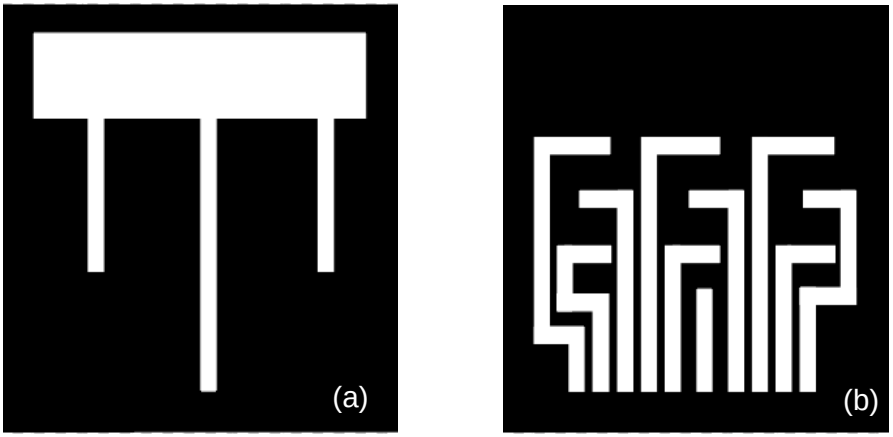

Figure 2.1 Mask design in Adobe Illustrator: (a) BE mask. (b) TE mask.

2.2 Device Fabrication

For the devices based on ITO/ZTO/Pt and Pt/ZTO/Ti-Au devices 2.5 x 2.5 cm^2 glass substrates (1737, Corning) were used as substrate while for ITO/GIO/Au device a 2.5 × 2.5 cm^2 commercial ITO.

The first step of the fabrication processes was to clean the impurities. The substrates were submerged in acetone solution for 10 minutes in an ultrasound bath followed by 10 min also in an ultrasonic bath of alcohol. After that, the substrates were washed with pure water and dried with nitrogen. Finally, the samples were heated for 10 min at 110 ºC to evaporate all of the water remaining.

2.2.1 ITO/ZTO/Pt

The ITO is the BE layer patterned by the previously referred BE shadow mask. The deposition was made via sputtering (AJA ATC-1800) using a target of ITO (90:10 wt.%, Super Conductor Materials, Inc., 99.99%) at a temperature of 200 ºC in the presence of a mixture of argon (20 sccm), oxygen (0.3 sccm) and nitrogen (0.3 sccm). The pressure

during the deposition was 2.30 × 10^{-3} Torr with a r.f power of 100 W, keeping a target substrate distance of 35 cm to deposit a 200 nm layer of ITO.

The next layer was also deposited via sputtering (AJA ATC-1800), where a ZTO ceramic target (1:1 weight fraction, AJA International, Inc.,99,99%) was used at room temperature (RT) in an atmosphere of equal amount of argon (20 sccm) and oxygen (20 sccm). The r.f. power was 160 W, the target distance of the substrate was 35 cm and the deposition occurred at a pressure of 2.3 × 10^{-6} bar. An 80 nm thick layer of ZTO was deposited. It was used the shadow mask represented in Figure 5.1 of Annex 1 only to pattern the layer.

The TE was deposited via electron-beam evaporation (homemade apparatus) being patterned by the TE shadow mask. The deposition was operated with a pressure of 8.25 × 10^{-9} bar, at RT. To get 60 nm of platinum, it was necessary to use a beam filament current of 1.50 × 10^{-4} A, using the common deposition parameters of the bulk density of 21.0 g.cm^{-3} and acoustic impedance (also known as z-factor) of 36.06 × 10^{5} g.cm^{-2}.s^{-1}.

2.2.2 Pt/ZTO/Ti-Au

In these devices to form the BE, a 30 nm thick titanium adhesion layer (to the glass substrate) and a 30 nm thick platinum layer were deposited via electron beam evaporation, with the pattern of BE shadow mask. This deposition was performed at a pressure of 1.12× 10^{-8} bar, at RT. A 30 nm thick layer of titanium was deposited, using a beam filament current of 7.0 × 10^{-5} A, using the common deposition parameters of the bulk density of 4.50 g.cm^{-3} and the acoustic impedance of 14.10 × 10^{5} g.cm^{-2}.s^{-1}. The Pt layer was deposited with the same parameters as the one in ITO/ZTO/Pt, but a 30 nm thick layer was deposited.

The ZTO layer followed the procedure described in the previous section.

For the last layer of these devices, the TE was patterned with the TE shadow mask using the same physical process in order to deposit 6 nm of titanium and 60 nm of gold. The Ti layer was deposited with the same parameters as the one in ITO/ZTO/Pt based devices. The gold was deposited with a pressure of 5.25 × 10^{-9} bar, at RT. To get 60 nm of gold it was used a beam filament current of 1.0 × 10^{-3} A, using the common deposition parameters of the bulk density of 19.30 g.cm^{-3} and acoustic impedance of 23.20 × 10^{5} g.cm^{-2}.s^{-1}.

2.2.3 ITO/GIO/Au

The ITO layer was commercially made.

A GIO layer was deposited via sputtering (AJA ATC-1300) on the commercial ITO substrate. Targets of In_2O_3 (AJA International, Inc.,99,99%) and Ga_2O_3 (AJA International, Inc.,99,99%) were used at RT, in a mixture of argon (14 sccm) and oxygen (2 sccm). The deposition occurred at a pressure of 2.2 × 10^{-6} bar with a r.f. power of 120W in the Gallium target and 40 W in the Indium target. The deposition time was 28:30 minutes to form a film of 30 nm thick.

Lastly, a film of 100 nm thick of gold was deposited via electron-beam evaporation using the BE shadow mask, also using the same parameters of the gold in the Ti-Au layer of Pt/ZTO/Ti-Au device.

2.3 Electrical Characterization

The electrical characterization of all of the devices was performed using Agilent 4155C a semiconductor parameter analyser that is connected to a Cascade Microtech M150 probe station, running the software Metrics ICS. Agilent was also connected to the XPS sample holder via two electrical feedthroughs, that allows the in-operando electrical characterization. Keithley 4200SCS is another utilized semiconductor characterization system that was connected to the Janis ST-500 probe station. All measurements in this work were electrically performed by applying voltage sweeps to the TE while keeping the BE grounded. The procedures realized in these electrical tests were: (1) Pristine state to study the uniformity of the devices in each sample, (2) electroforming test to change the pristine state to a conductive state.

2.4 In-depth XPS Chemical Characterization

Chemical composition of the layers and interface from the ITO/ZTO/Pt and ITO/IGO/Au was measured via XPS (Kratos Axis Supra). The detail spectres were acquired under an emission angle of 90° with a pass energy of 5 eV, resulting in an energy resolution better than 0.45 eV. XPS depth profiling was performed using a 5 keV argon monoatomic cluster gun energy to sputter the samples, in a raster size of 1 × 1 mm^2 centred on middle of the sub-devices for the ITO/ZTO/Pt sample. The depth profiling in ITO/GIO/Au sample was realized using the same argon cluster but using 10 keV energy of 500 argon atoms to sputter the samples, focusing on a raster size of 1,5 × 1,5 mm^2 centred on middle of the sub-devices. Samples were in the XPS vacuum chamber in pressures maintained below 10^{-11} bar.

2.4.1 Software analysis

The XPS spectra were analysed using CasaXPS software to calculate the atomic ratios and oxidation states. The background method applied to fit all the spectra was the Shirley background. The fitting to know the oxidation state is specific for each individual element, being necessary different line-shapes to fit correctly all the studied peaks. The Gaussian (70%) – Lorentzian (30%) lines-shapes, defined as GL (30) in the software, were used to fit the gallium element and GL (80) to fit the oxide components of indium's peaks in the GIO layer, in ITO/GIO/Au sample. On the other hand, the peaks of zinc, tin and titanium of the Pt/ZTO/Ti-Au sample were asymmetric. Also, the peaks of tin, the metal component of indium in GIO layer and the oxide component of the indium element present in the ITO layer from the ITO/GIO/Au sample, had an asymmetric peak. This asymmetry was defined in the software under the form of LA (α, β, m). *α* and *β* are used to specify the spread of the tail on the sides of the Lorentzian component. The parameter *m* defines the width of the Gaussian that convolutes with the Lorentzian curve. The parameters used to fit all these asymmetric peaks in the ITO/GIO/Au were LA (1.8,85,70). In the ITO/ZTO/Pt, LA (1.8,2,2) for tin and zinc and LA (1.1,5,7) for titanium were the ones that fitted the best with the asymmetric peaks.

3 Results and Discussion

This chapter will present the electrical and XPS analysis of the RS mechanisms of two fabricated devices, presented in two sub-chapters.

The first sub-chapter portrays the electrical memory behaviour of the Schottky barrier in the BE electrode of the Pt/ZTO/Ti-Au device. The second sub-chapter depicts the ITO/GIO/Au electrical trapping behaviour. The ionic movements between the semiconductor and the active electrode of both devices were analyzed realizing depth profiles in the XPS and by comparing the Low Resistive State (LRS) and the pristine state of each of both devices.

Figure 3.1 represents the final form of the 2.5 × 2.5 cm^2 samples fabricated and that will be further analyzed in this all chapter. Each sample has 9 sub-devices of 1 × 1 mm^2 electrodes overlapping area. This structure was designed to realize an electrical study of the devices inside the XPS, with a connection to a semiconductor parameter analyzer.

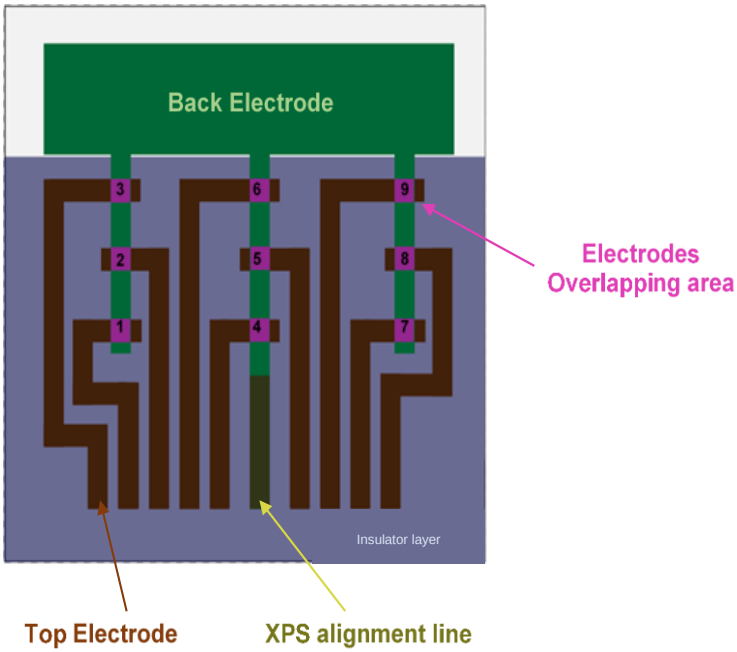

Figure 3.1 Structure of patterned samples with the enumeration of the sub-devices (electrodes overlapping area) of each sample, for electrical characterization.

3.1 Electrical and XPS Analysis of the RS mechanisms

3.1.1 Pt/ZTO/Ti-Au

This material composition of the layers was chosen following a previous master thesis of the same university's department [25]. The only difference is found in the reduction of thickness to 30 nm of the Platinum BE layer and in the thicker 30 nm of the Titanium adhesion layer, to ensure a better adhesion to the substrate. The main purpose of the choice of this device is that the electrical characterization procedure is well reported. Since the Schottky barrier is at the bottom of the device (interface between Pt and ZTO), a depth profiling approach was chosen. The novelty of the here reported results is that two different device states (pristine and LRS) were comparatively studied. Figure 3.2

shows that the Schottky barrier is at the bottom contact since the forward direction if in negative polarity

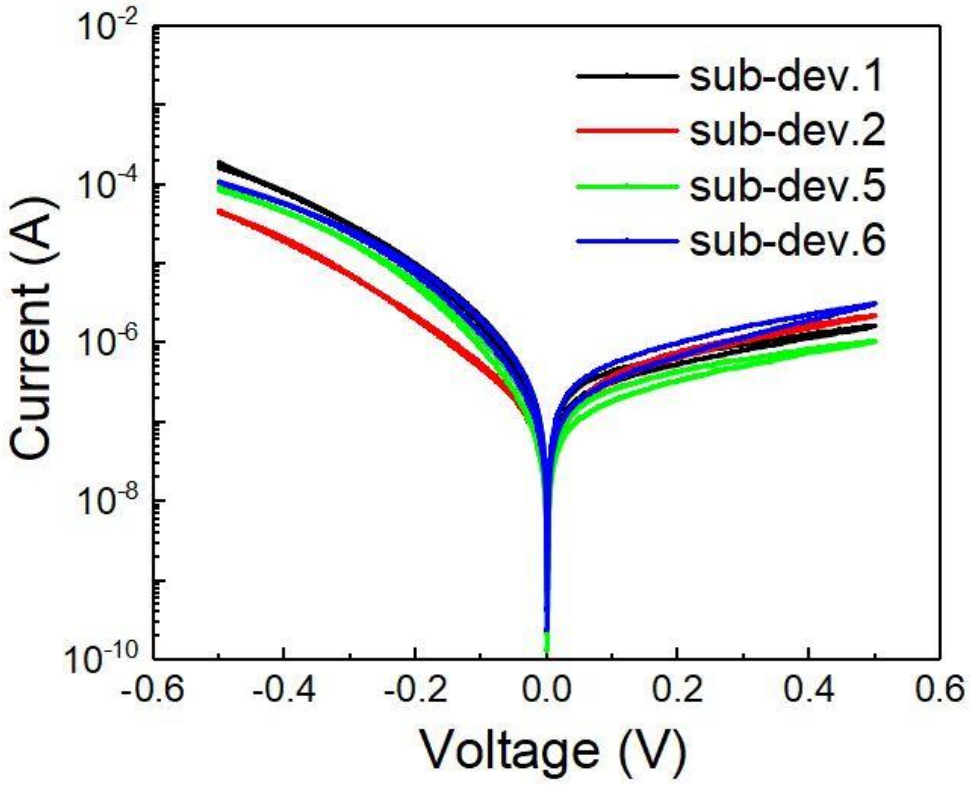

Figure 3.2 I-V characteristic comparison of pristine state of the sub-devices 1,2,5 e 6 of the TiPt/ZTO/TiAu sample.

Table 3.1 reveals the parameters that were used to perform the electrical measures to compare the pristine states of the sub-devices of Figure 3.2.

Table 3.1 Parameters of Pristine I-V characterization of TiPt/ZTO/TiAu sample.

Parameters of Pristine I-V Characterization :	**Voltage dual sweep from** − 0.5 V **to** 0.5 V
	Step: 0.002 V
	Number of Points: 1002
	Compliance: 0.1 A

It was selected the sub-device 2 to perform the electrical tests to analyse the resistive switching properties. The LRS was reached after a device initiation with a compliance of 2×10^{-2} A and applying 3.5 V in the forward polarity, represented in Figure 3.3 (a). This figure also portrays the Reset after the electroforming. The rectification is about 10^1 when compared with Set 2 performed without a CC. It's possible to observe in Figure 3.3 (b), that this ratio maintains after 50 cycles, but the hysteresis window of both polarities of the 50th cycle it's shortened when compared to the first cycle.

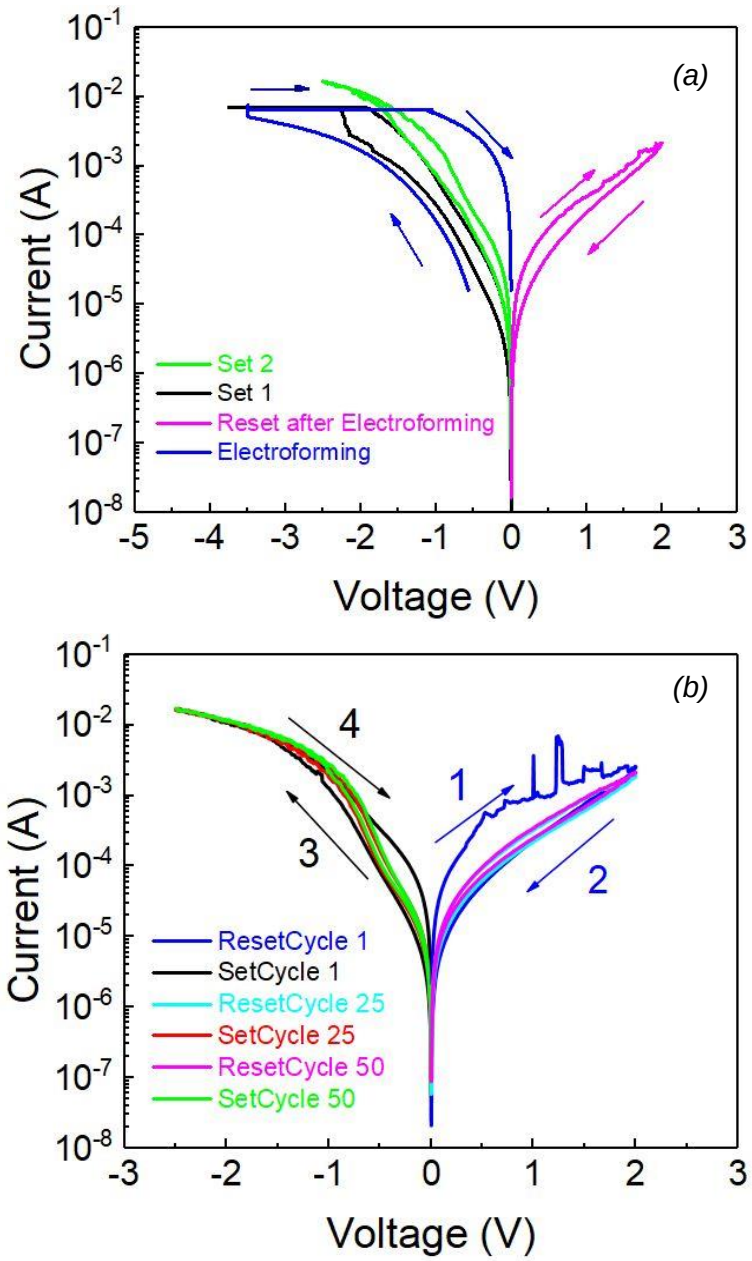

Figure 3.3 Bipolar resistive switching of the device 2 of Pt/ZTO/Ti-Au: (a) Electroforming, reset after performed the electroforming and two set tests before the cycles, (b) 50 consecutive cycles of both Set and Reset.

The last electrical test of the sub-device 2 in the semiconductor parameter analyzer was the Set cycle 50. The resistance between the contacts when placed on the designated holder of the XPS was tested with a multimeter, to confirm that the LRS wasn't lost during the transfer process. Table 3.2 Table 3.2 Resistance values of the sub-devices 2 and 6 when mounted in the XPS holder, outside the XPS and inside the main chamber compared to the theoretical value from the linear regression.shows the resistance values between the contacts before the XPS analysis and when it's inside of the XPS main chamber comparing with the resistance value calculated from the linear regression of the last reset cycle performed from 0 to 0.2 V (range of values used by the multimeter to determine the resistance value). So, the resistance value of the linear regression of the last reset can be assumed as the LRS resistance value of the sub-

device 2. This table also shows the resistance values of the sub-device 6 that was in Pristine when introduced in the flexi-lock of the XPS.

Table 3.2 Resistance values of the sub-devices 2 and 6 when mounted in the XPS holder, outside the XPS and inside the main chamber compared to the theoretical value from the linear regression.

LRS Resistance value of sub-device 2: 1 kΩ	**Resistance Value Before XPS:** 1.3 kΩ
	Resistance Value in XPS main chamber: 1.1 kΩ
Pristine Resistance value of sub-device 6 : 210 kΩ	**Resistance Value Before XPS:** 209 kΩ
	Resistance Value in XPS main chamber: 210 kΩ

After confirmed that the states are preserved when introduced into the XPS, they now can be submitted to a depth profile test. The depth profile tests allow obtaining information of the elements in the different layers of the sample, using a controlled erosion of the surface by ion sputtering [19]. Figure 3.4 represents the atomic concentration of the elements of the sample, in each etch step in both the LRS and Pristine devices.

Pristine

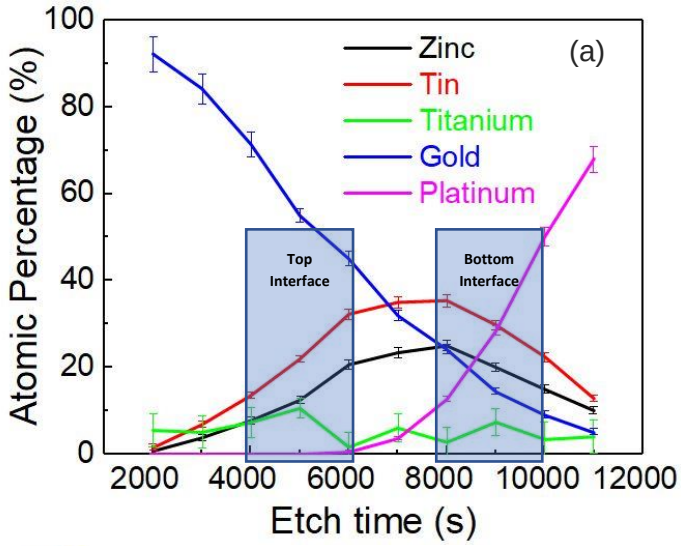

LRS

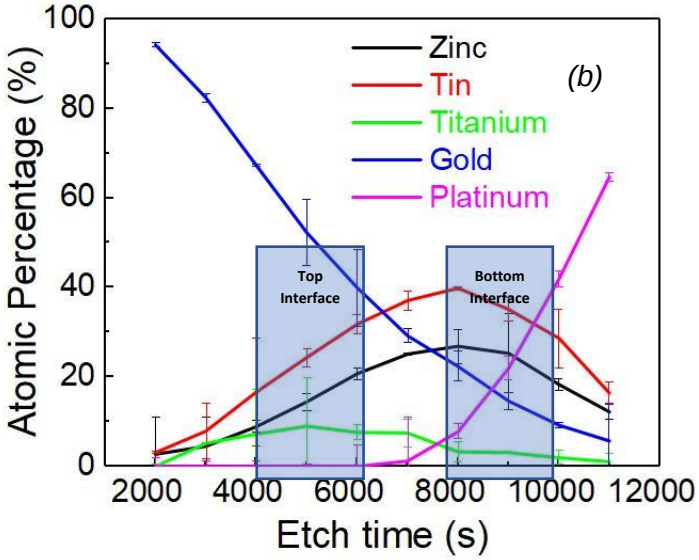

Figure 3.4 Atomic concentration of the (a) Pristine and (b) LRS sub-devices of the Pt/ZTO/Ti-Au per etch time realized by the sputtering inside the XPS system.

Figure 3.4 (a) and (b) shows, that the transition from the gold and titanium layer to the ZTO layer began in the 2000 s etch time where the gold concentration begins to decrease and the atomic concentration of tin, zinc and titanium increase. The transition finished after the 6000 s etching where a drop of the Ti atomic concentration is observed, indicating the start of the etching of the ZTO layer. The transition of the ZTO to the Platinum appears to start happening in the 8000 s etch time and finishing in the 11000 s etch time, where the Pt atomic concentration increased remarkably and in contrast, the concentrations of the other elements decreased appreciably.

A study of the oxide and metal components of the elements, from the XPS data, present in the sample was realized by deconvoluting the peaks using mixed Gaussian-Lorentzian profiles over a Shirley background. The components of the elements between the 2000s and 5000s etch time are represented in Figure 3.5. The full lines represent the measured data. In the dashed red lines are represented the oxide state of the elements and the metallic state is portrayed by the green dashed lines. The etching time is indicated on the z-axis.

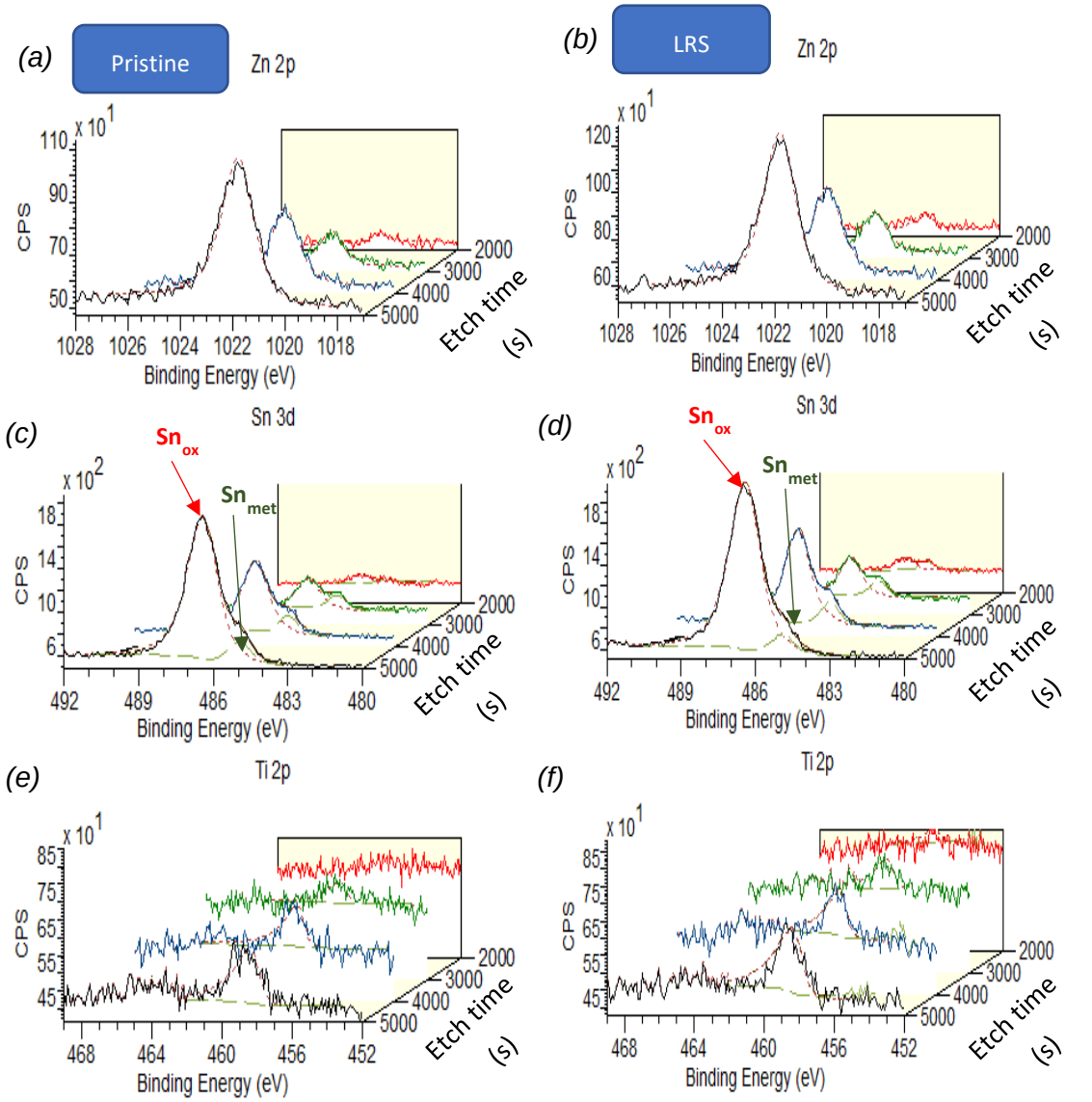

Figure 3.5 XPS 3D spectra of depth profiling on the Ti/ZTO transition etch times, showing the main emission of (a) zinc , (c) tin and (e) titanium of the pristine state device. Also represented the same main emission and etch times of (b) zin, (d) tin and (f) titanium of the LRS sub-device.

The spectra of the zinc and titanium are presented in Figure 3.5 (a) and (b) for zinc, and (e) and (f) for titanium. The peaks of the Zn $2p_{3/2}$ and Ti $2p_{3/2}$ are both well described in a single component fitting (LA (1.8,2,2), LA (1.1,5,7) respectively) for each element. In the case of Zn $2p_{3/2,}$ it's hard to define the state of the component due to the small chemical shift in the binding energy between the metallic Zn^0 and the oxide Zn^{2+}, both centred around 1022 eV binding energy. [19] The Ti $2p_{3/2}$ peak suggests that the element is fully oxidized because a single component with a binding energy position of 458.5 eV is situated in the binding energy range of the Ti^{2+} or Ti^{4+} oxidation states. [19]

The situation of $Sn3d_{3/2}$ is different, the emission is composed by 2 components fittings (both LA (1.8,2,2)), the oxide component of Sn^{2+} or Sn^{4+} (in the range of 486-487eV) and the metallic component Sn^0 (around 485 eV). Figures 3.5 (c) and (d) an intensity reduction of the tin metallic component is shown when increasing the etch time. This indicates that a higher amount of reduced tin is present closer to the Ti interface, compared to the platinum interface. A bigger concentration of Sn metallic state appears due to the oxygen-getter effect by the titanium layer. [26]

Figure 3.6 illustrates the behaviour of the components of zinc (a) and (b), tin (c) and (d), and platinum (e) and (f) from the 8000 s etch time to the 11000 s etch time.

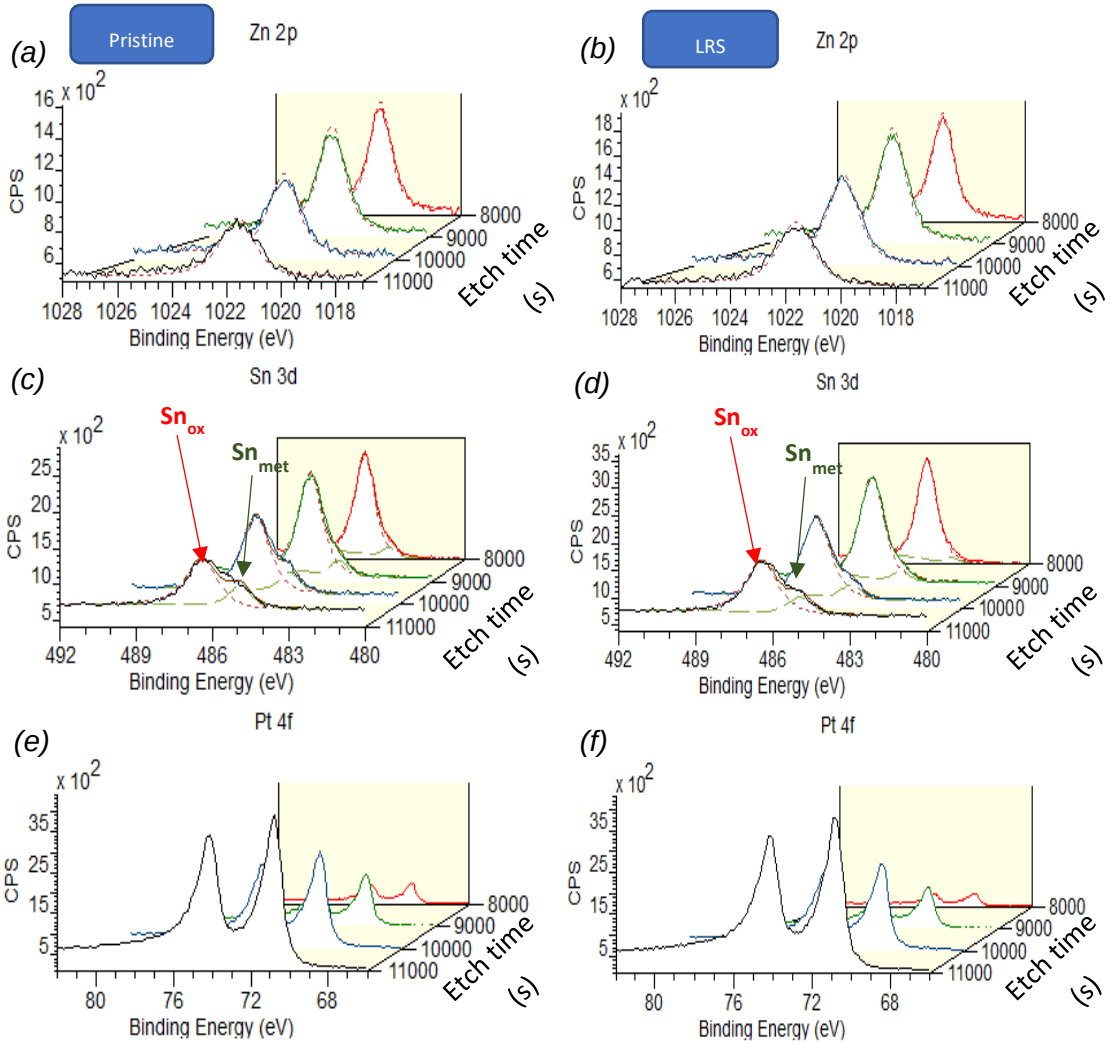

Figure 3.6 XPS 3D spectra of depth profiling on the Pt/ZTO transition etch times, showing the main emission of (a) zinc, (c) tin and (e) platinum of the pristine state device. Also represented the same main emission and etch times of (b) zin, (d) tin and (f) platinum of the LRS sub-device.

The Zn $2p_{3/2}$ component in the Pt/ZTO transition etch times follows the behaviour of the component in the transitional etch times from the Titanium to the ZTO, same peak position of the binding energy only varying the counts per second values for each etch time. The Pt 4_f also has the stability of the binding energy positions 71 and 74 eV (this energy values are from the $4f_{5/2}$ and $4f_{7/2}$ emissions, respectively) for the various etch times and there are no detectable signals of a platinum oxide component. The behaviour of the components of the $Sn3d_{3/2}$ in this interface Pt/ZTO is just the same as the Ti/ZTO transition etch times, observed again the increase of the metallic component concentration near the platinum. [27]

It was noticed a slight difference of the metallic component of the $Sn3d_{3/2}$ area percentage between the pristine and the LRS state in both electrode interfaces. For that reason, the atomic ratio based in atomic percentages of Sn_{met}/Sn_{oxi} and the atomic ratio of Sn/Zn was analysed in Figure 3.7, in both LRS and Pristine state, respectively.

The atomic percentage of the components of the elements (also represented in Figure 3.4) was calculated via CasaXPS using the following formula:

$$\text{at.}\,\%\,(\text{i}) = \frac{N_{\text{i}}}{(N_{\text{tot}})} \times 100\,\%, \tag{3.1}$$

Where *i* is the component that is being studied, N_i is a result given by the software CasaXPS, that represents the fitting of the component *i* with the element peak and N_{tot} is the total of the values of the fitting representations of all the components analysed.

In Figure 3.7 (a) Figure 3.7 (b) are shown the atomic ratio of Sn_{met}/Sn_{oxi} that was calculated using the atomic percentage of the components of the formula:

$$\text{A}_{Sn\ met\ /Sn\ oxi} = \frac{(at.\%\ Sn_{\ 3d\ metal})}{at.\%\ Sn_{\ \text{3d oxide}}} \tag{3.2}$$

Also in these figures are portrayed the Sn/Zn atomic ratio and was calculated using the atomic percentage of the components of the formula:

$$\text{A}_{Sn/In} = \frac{Sn_{\ 3d}}{(Zn_{\ 2p})} \tag{3.3}$$

In Figure 3.7 (a) the atomic ratios of Sn^0/Sn^{x+} are in the function of gold atomic percentage to see the behaviour near the top interface. In Figure 3.7 (b) the atomic ratios are the in function of platinum atomic percentage to compare the chemical characteristic near the bottom interface.

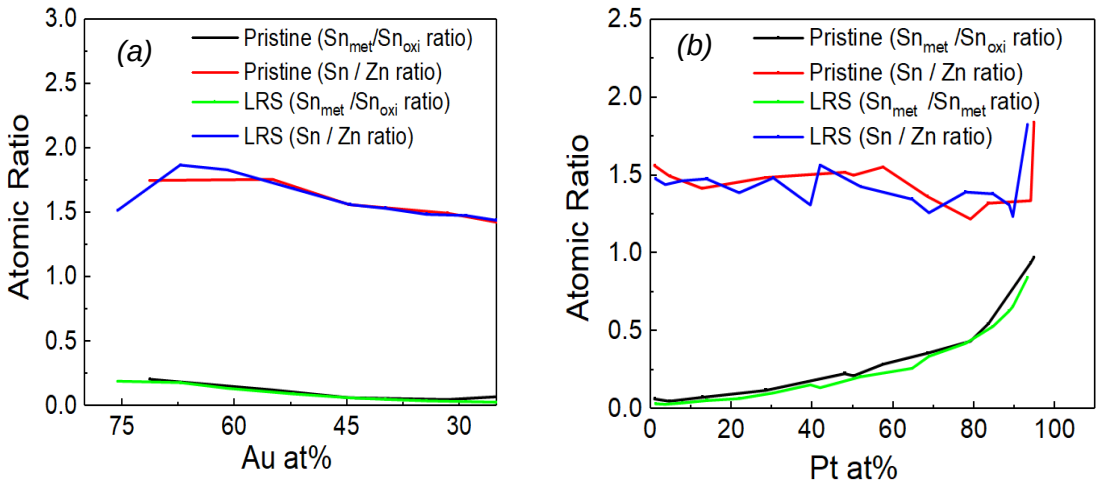

Figure 3.7 Atomic ratio of the metal to oxide component of tin and atomic ratio of tin to zinc, in both LRS and Pristine state, in function (a) of gold atomic percentage and (b) of platinum atomic percentage.

Both in Figure 3.7 (a) and Figure 3.7 (b), no evident change in the atomic ratios nor in the chemical state of tin between the LRS and pristine state is observed. For the interpretation of this observation, it is taken into consideration an area-dependent mechanism is causing the resistive switching, based on previous results. [25] Hence, the RS mechanism has to be purely electronic, since the graphs of the LRS and pristine states exhibit no chemical difference. The behaviour of the atomic ratios of the metal to oxide components in both states are nearly overlapped in the ZTO layer and near both interfaces of the device. If the RS mechanism were due to cationic movement or due to redox reactions, there should be a bigger and explicit difference in both states. That difference would represent the redox reactions in the interfaces and the stoichiometric

change in the elements that happen during the resistive switching process. The conclusion of a purely electronic switching mechanism is in line with a recent report from literature, in which area-dependent switching in which several oxide-based devices with a platinum electrode were compared, leading to the same conclusion as drawn from the here presented in-depth XPS analysis. [28]

3.1.2 ITO/GIO/Au

A structure ITO/ZTO/Pt was the first device fabricated in this work, due to having the TE working as the AE, a characteristic required for the intended in-operando approach. The electrical measurements in Annex 3 shows uneven pristine states (needed to compare the results of the different resistive states) and barely a resistive switching in these ITO/ZTO/Pt devices. Only later was checked in the literature that these devices do not switch the resistance. [25] In a parallel activity during the thesis work, ITO/GIO/Au devices were being studied, to work as diodes based on gallium-indium oxide with a gold top-electrode forming a Schottky junction, by a visiting researcher (Hasan Arif Yetkin, HZB Berlin). Having the Schottky junction as the top contact made these devices appealing for the in-operando approach, and, more importantly, they presented interesting hysteretic IV-curve, which were interesting to be explored further. Furthermore, some initial studies in literature about the GIO as an insulant layer were found for resistive memory applications. [29] ITO was used as ohmic contact in BE and Au as Schottky contact in TE. Electrical tests realized in the semiconductor parameter analyzers outside the XPS are represented in Figure 3.8 The pristine state graph (Figure 3.8 (a)) and the pristine state comparison with the state after performing an I-V characteristic from the 0 V to 8 V dual sweep (Figure 3.8 (f)), were realized under the parameters represented in Table 3.3.

Table 3.3 I-V characteristics of pristine state and pristine comparison after an 11V dual sweep of the sub-device 1 of ITO/GIO/Au sample.

Parameters of Pristine state and Pristine comparison I-V Characterization :	**Voltage dual sweep from** − 0.5 V **to** 0.5 V
	Step: 0.005 V
	Number of Points: 402
	Compliance: 0.1 A

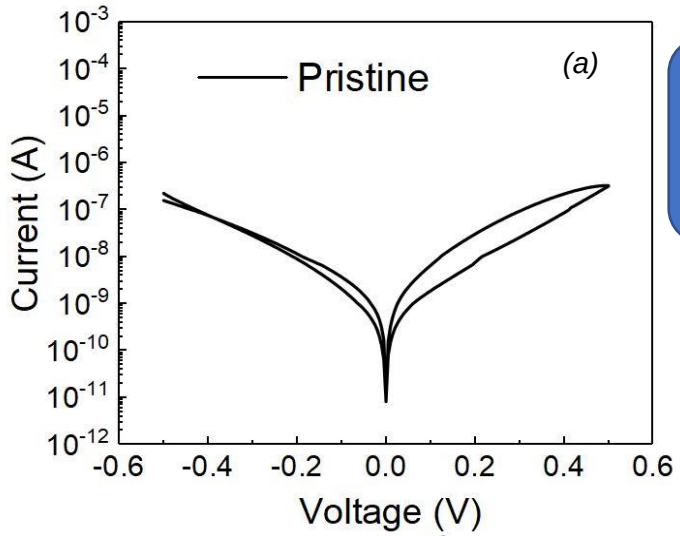

Electroforming outside XPS

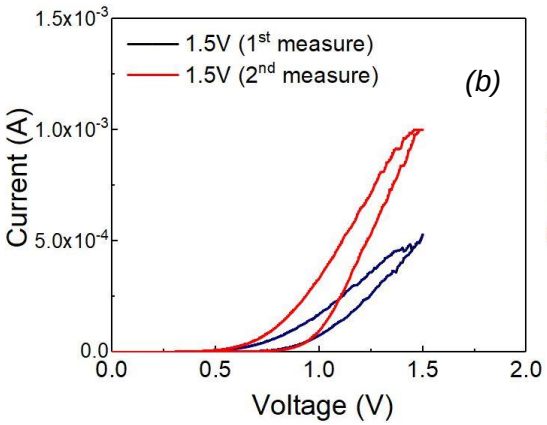

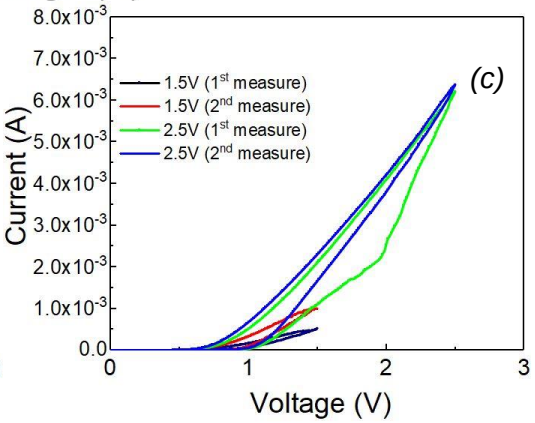

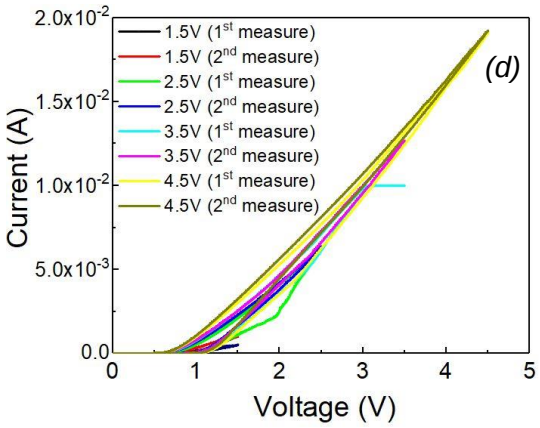

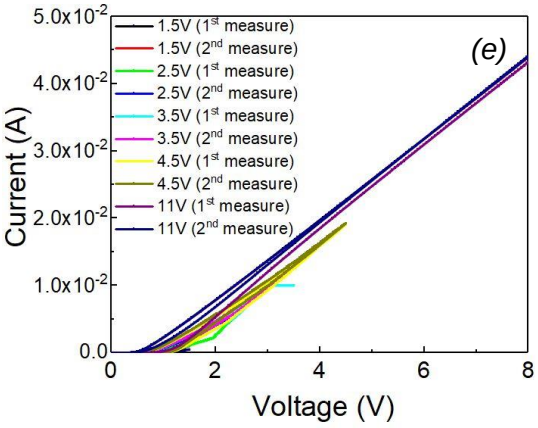

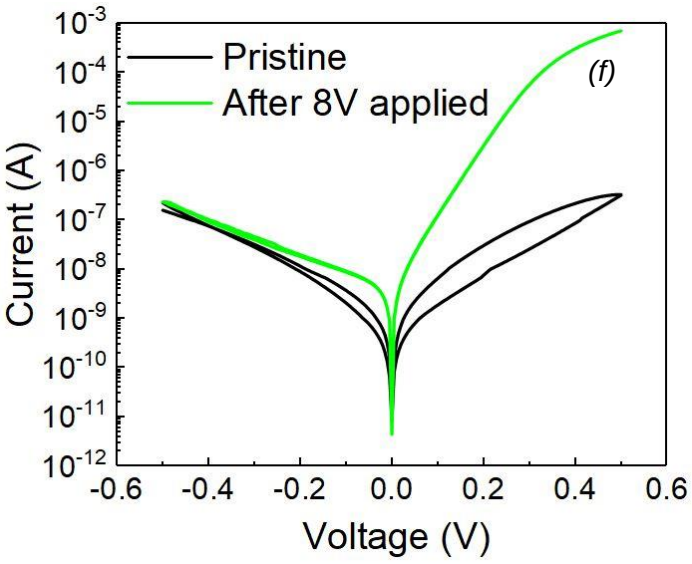

Figure 3.8 I-V characteristics of the sub-device 1 of ITO/GIO/Au Sample: (a) Pristine state, (b) I-V from 0 V to 1.5 V dual sweep, (c) I-V from 0 V to 2.5 V dual sweep compared to the previous graph, (d) I-V from 0 V to 4.5 V dual sweep compared to the previous graph, (e) I-V from 0 V to 11 V dual sweep compared to all the previous sweeps, (f) I-V comparison between the Pristine state and the state after the 11V dual sweep.

The device represented in Figure 3.8 showed a hysteresis in the pristine state and a gradual increase forward current when cycled repetitively. The device was submitted to a gradual dual sweep I-V increasing voltage from 1.5 V to 8 V, represented in order by the Figure 3.8 (b), (c), (d) e (e). This is similar to gradual resistive switching behaviour observed in other gallium oxide-based devices. [10] However, the ITO/GIO/Au devices could not be reset remaining in an irreversible permanent resistance state after applied the progressive voltage. Instead of showing resistive switching, the devices could be gradually electroformed, to a state of significantly improved rectification with a lack of any hysteresis. For this reason, an in-depth XPS analysis was realized, because it is expected that can give very important chemical information. It was analysed the chemical differences between the material in pristine state compared to the rectifier diode formed after the electroforming.

3.1.2.1 In-depth XPS characterization

A novel in-operando approach for electrical characterization was done for the first time inside the main chamber of the XPS, at an Ultra High Vacuum. It was used the same procedure of the previous electrical characterization that was done to obtain the diode behaviour, but this time applying the voltage with the sample already inside of the main chamber of the XPS.

Figure 3.9 (a) shows the pristine states of the sub-devices 4 and 6 analysed outside the XPS.

Figure 3.9 (b), (c), (d) and (e) shows the electrical characteristics when applying up to -6.5 V on the sample.

Figure 3.9 (f) portrays the difference between the pristine state measured in-operando of one sub-device and the diode behaviour shown by the sub-device after applied the -6.5V.

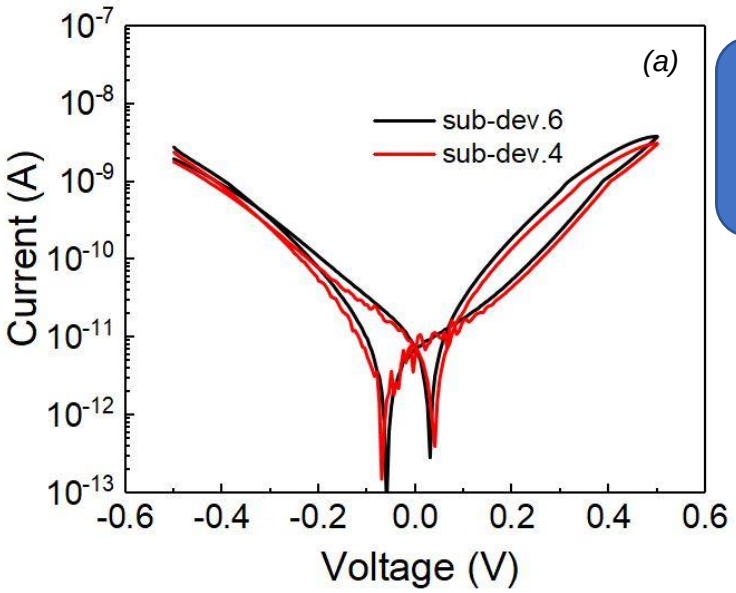

Electroforming inside XPS

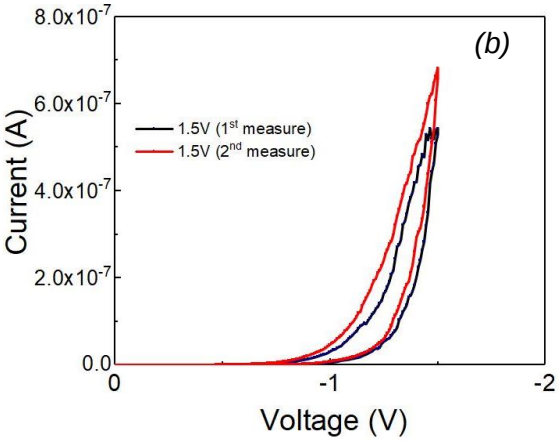

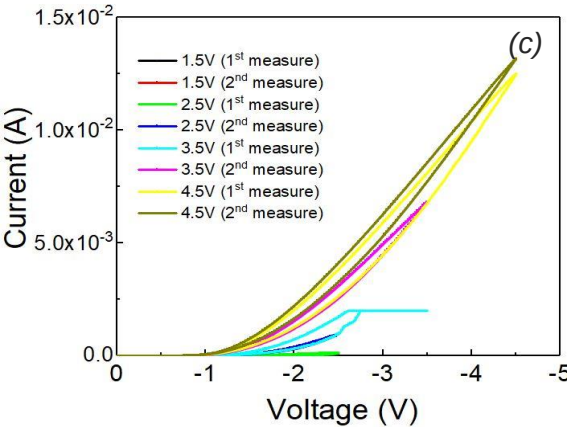

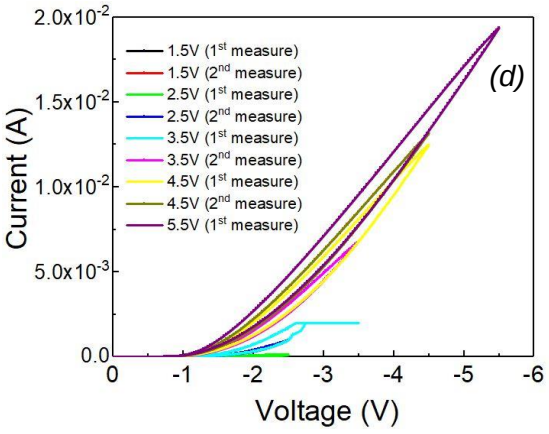

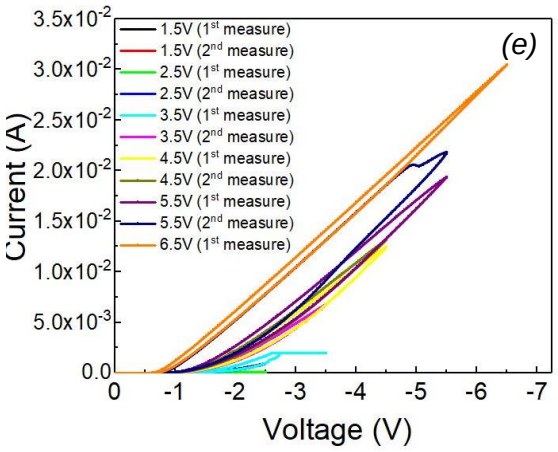

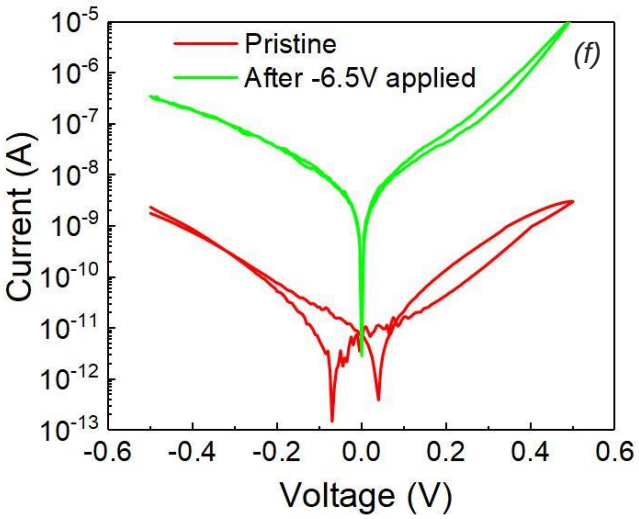

Figure 3.9 In-operando electrical characterization of the ITO/IGO/Au sample : (a) Comparison between the pristine states realized outside the XPS of the sub-device 6 and 4. (b) I-V from 0 V to 1.5 V dual sweep, (c) I-V from 0 V to 2.5 V dual sweep compared to the previous graph, (d) I-V from 0 V to 4.5 V dual sweep compared to the previous graph, (e) I-V from 0 V to 6.5 V dual sweep compared to all the previous sweeps, (f) I-V comparison between the Pristine state measured in-operando and the diode behaviour state after the 6.5 V dual sweep.

In this in-operando electrical characterization, it was applied voltage in the BE and the TE was grounded (reverse bias) to prevent short-circuits and some leakage current that can affect the resistivity of the sample by accumulation of electrical particles in the surface. That's the reason Figure 3.9 (b), (c), (d) and (e) shows I-V dual sweeps in the negative. It was observed a slight decrease in the current from the pristine performed outside of the XPS compared to the pristine done inside the main chamber of the XPS. Also, the rectification of about 10^2 was not so pronounced inside of the XPS (Figure 3.9 (f)) as the one analysed outside of about 10^4 (Figure 3.8 (f)).

An XPS depth profile was realized in 2 the sub-devices to understand if occurred a significantly chemical difference in the elements between the pristine state and the diode state. Figure 3.10 (a) determines the atomic concentration of the elements present in the Pristine in-depth state sub-device of Figure 3.9 (f) for each etch step. The same applies to Figure 3.10 (b) but analysing the sub-device that shows the diode rectification. The temporal step of each etch in this depth profile was 360 s after a 5000 s continuous sputtering to etch the majority of the Au TE layer.

Pristine

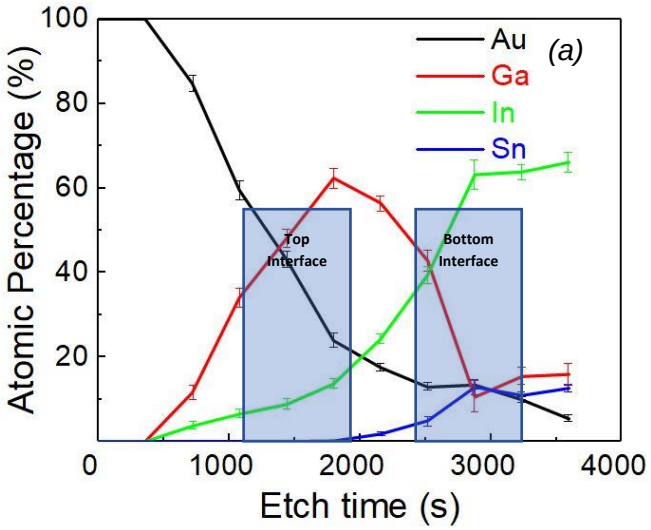

Rectified

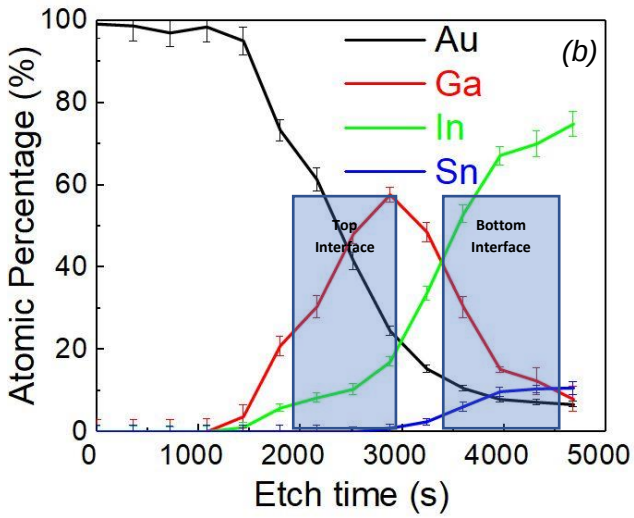

Figure 3.10 Atomic concentration of the (a) Pristine and (b) Rectified state sub-devices of the ITO/IGO/Au per etch time realized by the sputtering of the XPS.

The first difference noticed in the graphs of Figure 3.10 is that the gold concentration of (b) stays around 100% for about 1080 s longer than Figure 3.10

(a). This means that it took more time, around 2 more etch steps, to etch the gold and reach the IGO layer in the sub-device of Figure 3.10(b), possibly due to some difference in the thickness of the gold during the electron beam evaporation.

So, for the study of the components, illustrated in Figure 3.11 and in the Figure 3.12, was required normalization of the etch times between the Pristine and the diode behaviour XPS analysis. The 0 value of the normalization will correspond to the 720s etch time of the pristine graph, and to the 1800s etch time of the sub-device with the diode behaviour.

Figure 3.11 has represented the chemical components of the three elements of the Au/IGO interface. The first detail to have into account is the binding energy discrepancy of about 3 eV between the graphs of the pristine state and the diode state. The diode state graphs show the correct representation of the binding energies values, for example, the gold peak should be in the 84 eV binding energy and that can be observed in the Figure 3.11 (f). This could be fixed realizing a calibration in the software, but the main focus of this analysis is the concentrations and ratios of the metallic and oxide components of each element. So, the peak position of the binding energies used as a reference for each element is given by the diode state graphs.

The gallium and gold are defined with only one component in both states, in the case of the gallium is the oxide component with the peak position of the binding energy being around 1118 eV value.

The gold has a metallic state represented in the peak position value previously stated as 84 eV.

The indium element has two components, an oxide component and a metallic component. The oxide component is the most intense in this interface with the peak being represented in the 445 eV binding energy. The metallic component (with the peak position of 443-444 eV binding energy) concentration compared to the oxide component decreases with the increase of etch steps.

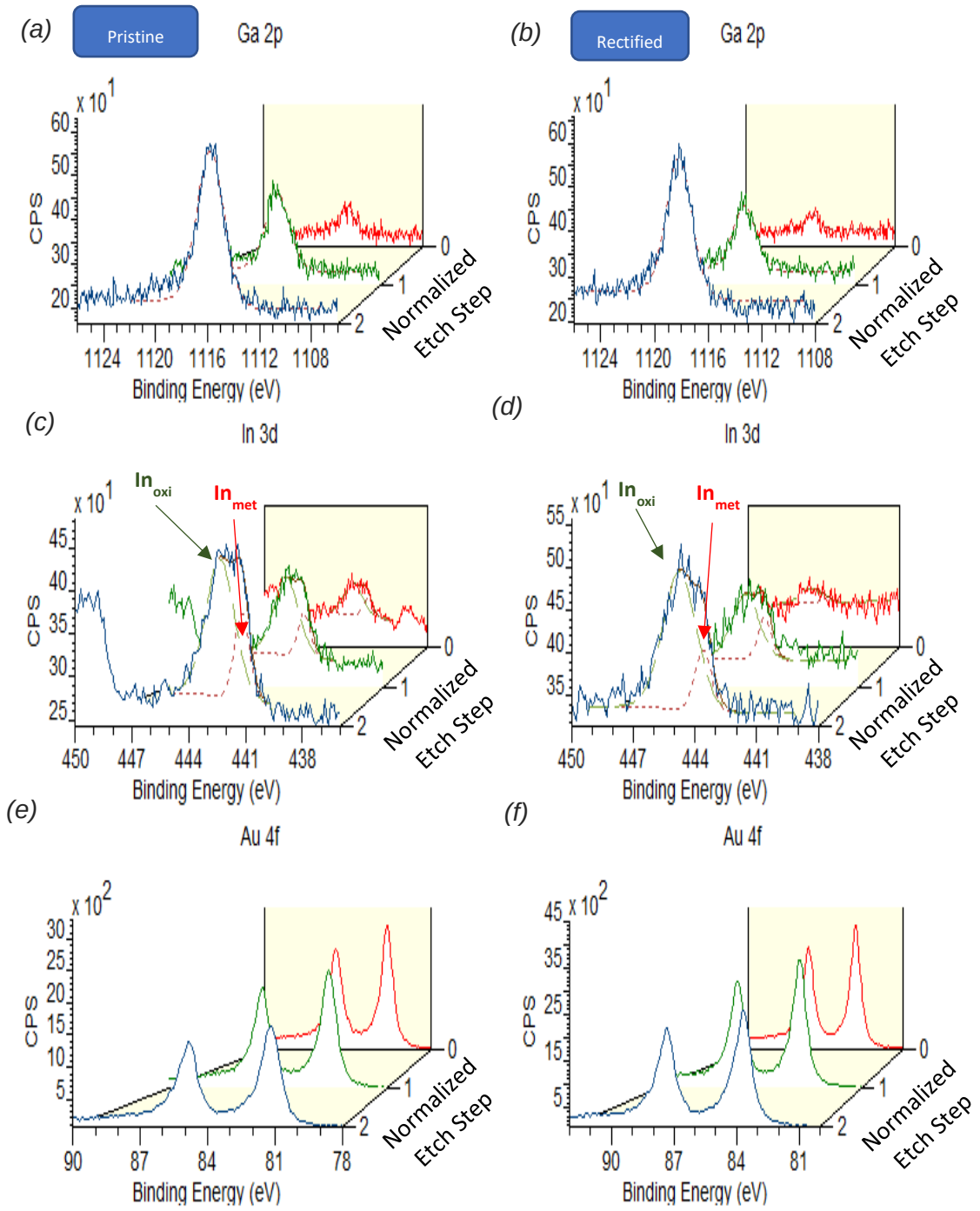

Figure 3.11 XPS 3D spectra of depth profiling on the Au/IGO transition normalized etch times, showing the main emission of (a) gallium, (c) indium and (e) gold of the pristine state device. Also represented the same main emission and normalized etch times of (b) gallium, (d) indium and (f) gold of the sub-device that shows a diode behaviour.

Moving to the bottom interface, the IGO/ ITO interface depth profile and components analysis is represented in Figure 3.12.

As the top interface, the diode state graphs of this interface are the reference to check in the literature which of the metallic or oxide components are represented in the peaks of the XPS analysis. But in both states can be observed the stability of the peak position and the concentration between the components for the different etch times of the interface when two or even three components appear in the element.

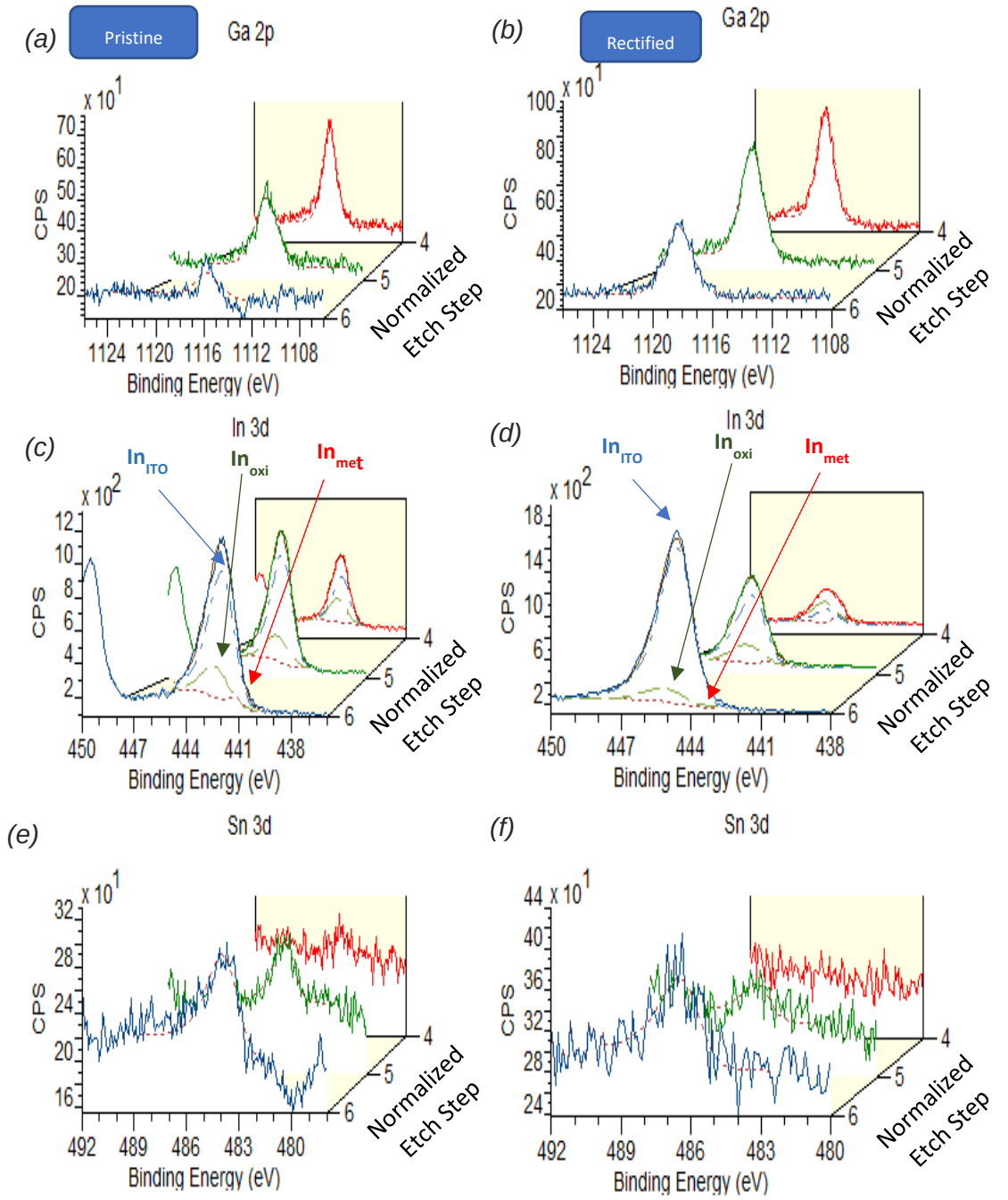

Figure 3.12 XPS 3D spectra of depth profiling on the IGO/ITO transition normalized etch times, showing the main emission of (a) gallium, (c) indium and (e) tin of the pristine state device. Also represented the same main emission and normalized etch times of (b) gallium, (d) indium and (f) tin of the sub-device that shows a diode behaviour.

The three elements studied in Figure 3.12 are the gallium from the IGO layer, the tin of the ITO layer, and the indium that is used as an element of both layers.

The gallium peak position of the binding energy as the same behaviour and position as studied in the previously studied interface, having only one oxide component.

The tin element present in this bottom interface gradually increases the intensity of the peak in both states (represented in the Figure 3.12 (e) and (f)) as the etch time also increases in both states. This makes sense because the bigger the etch step is, closer to the ITO bottom layer the analysis is being performed and more tin is interacting with x-rays. This tin element is represented with an oxide component, the peak position of the

energy binding corresponds to the values reported in literature of about 486-487 eV for the oxide's components of this element.

Lastly, was studied the components present in the indium element. This element has 3 components in this interface, because it is present in both of the layers that constitute the IGO/ITO interface, and for that reason is considered the influence of the structure of the ITO layer that the indium is included, in the components of the indium present in the IGO layer. The dashed red line of the Figure 3.12 (c) and (d) represent the metallic component of the indium around the binding energy value of 443-444 eV and is possible to observe that is close to 0 the peak intensity of this component. The dashed blue line illustrates the oxide component of the indium, with a peak position of the binding energy of 445 eV, with the influence of the structure from the ITO. It was used in this component the same line-shape to represent the tin component. The dashed green line portrays the oxide component of the indium without being influenced by the ITO layer and with the line-shapes of the gallium.

As expected, with the etch step getting bigger and closer to the ITO layer, the component concentration of the oxide component of the indium not influenced by the ITO layer is decreasing and the other component of this element represented by using the tin line-shape is increasing to be the dominant component.

After examined the behaviour of the peaks and the chemical state of the components, it was compared the percentage of indium compared to gallium and tin, in the IGO and ITO layers. Also, it was analysed the metal and oxide components of the indium components.

Figure 3.13 (a) shows the atomic percentage comparison between the metal component of indium to the oxide component, in the function of the gold percentage. The atomic ratio was calculated by:

$$\mathrm{A}_{\mathrm{In}_{metal}/\mathrm{In}_{oxide}} = \frac{(at.\%\ In_{\ 3d\ metal})}{(\mathrm{at.\%}\ In_{\ 3d\ oxide})} \tag{3.4}$$

Figure 3.13 (b) are represented the atomic ratios of gallium to indium in the function of gold atomic percentage throughout the device but giving more relevance near the interface of the Au layer in the IGO layer. These ratios were calculated using the atomic percentage of the components of the formula:

$$\mathrm{A}_{Ga/In} = \frac{(at.\%\ In_{\ 3d\ metal} + \mathrm{at.\%}\ In_{\ 3d\ oxide})}{at.\%\ Ga_{\ 2p}} \tag{3.5}$$

Figure 3.13 (c) has represented the atomic ratios of tin to indium in the function of gold atomic percentage for the transition from the IGO layer to the ITO layer. These atomic ratios were calculated using the atomic percent of the components of the formula:

$$\mathrm{A}_{Sn/In} = \frac{Sn_{\ 3d}}{(In_{\ 3d\ ITO})} \tag{3.6}$$

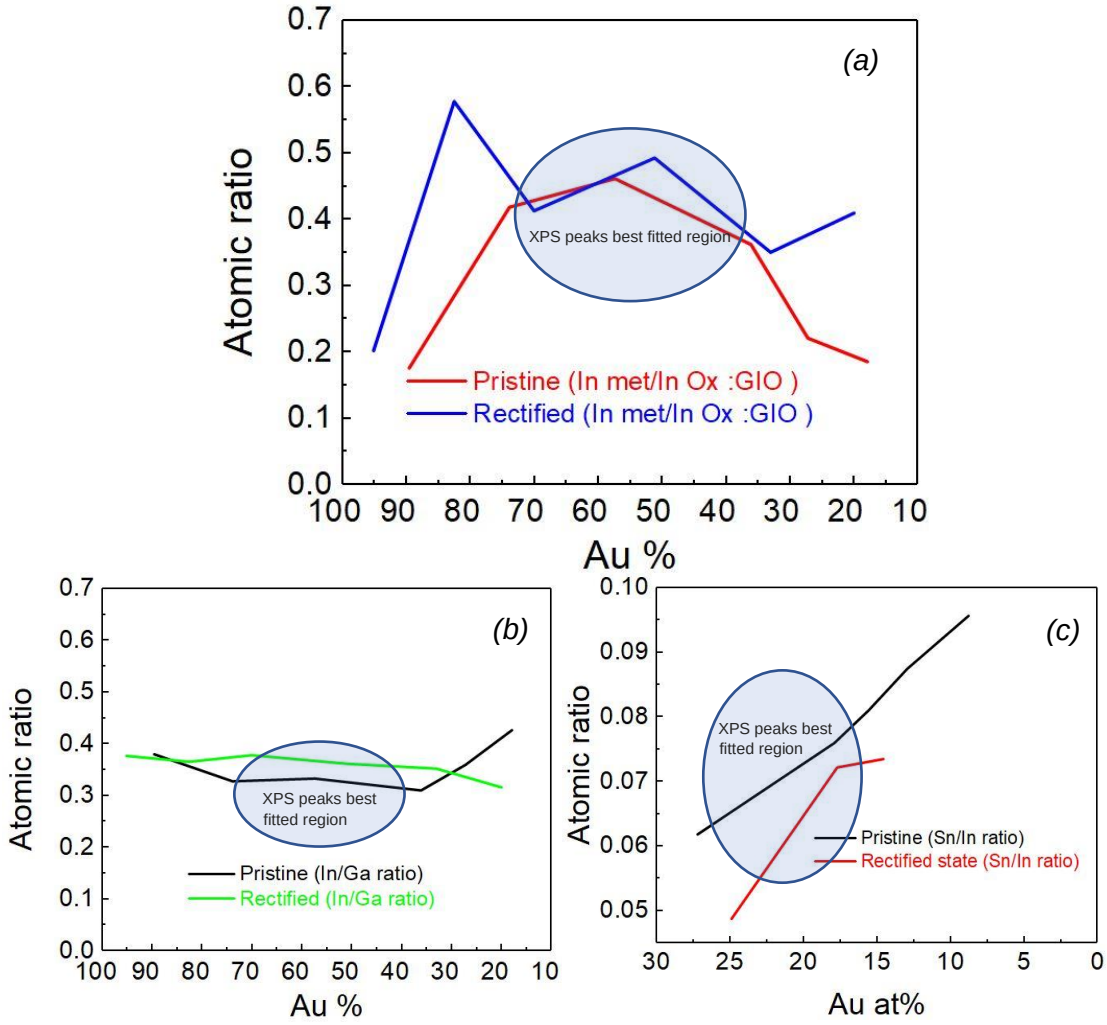

Figure 3.13 (a) Atomic ratio of metal components to oxide components of indium and (b) the atomic ratio of Indium to Gallium present in the GIO layer, in both diode and pristine state, in function of gold atomic percentage. (c) Atomic ratio of tin to indium, in the pristine and diode state, also in function of gold atomic percentage.

In Figure 3.13 the blue oval shape illustrates the zones of the atomic ratios where the fittings of the software best represented the shape of the peak and components. Also, in Figure 3.13 is showed that there is almost no difference in both ratios of the pristine state and diode state, but near the bottom interface, it's a slight difference in the atomic ratio of the tin to Indium. This difference indicates more indium in the diode state than the pristine state which it's in concordance with the simulation parameters included in Table 0.2. The simulation was based on an equation developed from Werner, that represents the physical parameters, illustrated in Table 3.4, that describe the behaviour of a diode. [30] Werner reached the following equation:

$$I = Id + Ip = Is\left(exp\left(\frac{\beta}{n}(V - IRs)\right) - 1\right) + Gp(V - IRs) \quad (3.7)$$

Where Id is the diode current and Ip describes the shunt current through a possible parallel conductance, Is is the saturation current, β = e/kT is the inverse thermal voltage, n is the ideality factor Gp with the resistance Rp=1/Gp, V and I are the voltage and current applied in the p-n junction.

Table 3.4 Parameters of simulation of the pristine and diode state.

	b (eV)	n	Rs (Ohm)	Rp (Ohm)
Pristine State	0.79	2.61	3.53×10^5	1.56×10^8
Diode State	0.74	1.29	1.80×10^2	3.81×10^4

The table portrays that the major changes happen in the values of the series and parallel resistances of the device and consequently affects the ideality factor of the diode, *n*. The values of the series resistance have a difference of some orders of magnitude that indicate the doping changes occurring in the bulk. The difference in the atomic ratio of the tin to indium near and in the ITO proves that's happening a stoichiometric change in the tin and indium elements due to that doping alterations in the bulk elements. The value of the barrier from the pristine to the diode state stays roughly the same, explaining the similarity of the atomic ratio values inside the GIO layer in the two states of the device.

So, despite some differences were observed in the electroforming realized inside and outside the XPS, such as, higher current in the reverse direction of the device electroformed inside the XPS due to some shunt resistance from the electrical system of the XPS. Other visible difference is still present some hysteresis in the analysed device inside of the XPS, the device electroformed outside of the XPS show no hysteresis.

Still, it was analysed and observed the effects of the sample electroformed inside of the XPS that lead to the loss of hysteresis due to the ionic movement of indium between the GIO layer and the ITO layer in the bulk region near the bottom interface. Also, it was noticed that the rectified state leads to improved series and parallel resistance and ideality factor of the diode

4 Conclusions and Future Perspectives

4.1 Conclusions

MIM structure's devices, Pt/ZTO/Ti-Au and ITO/GIO/Au were fabricated and accomplish a prominent change from the resistance state to a conductive state when applying voltage bias in the forward direction. The first sample mentioned (Pt/ZTO/Ti-Au) showed device initiation when applying −3.5 V of LRS and it was possible to reset the resistance state. The second sample (ITO/GIO/Au), after being submitted to an electroforming of 8 V, showed a distinguished change in I-V behaviour or improved diode characteristics and no hysteresis.

Chemical properties were properly analysed using the XPS argon cluster depth profiling method and used to explain and correlate the resistive mechanism occurring in the electrical procedure of each one of the devices:

I. The Pt/ZTO/Ti-Au exhibited a very similar area-dependent analog switching present in the reset process and a threshold set process, just like the device reported in literature. [25] XPS peaks displayed identical behaviour and relative intensities when comparing both pristine and LRS states. Consequently, no noticeable change happened to the cationic ratios and oxidation states calculated using the XPS spectra. This chemical resemblance in the oxidations states indicates that the RS mechanism was not due to ionic movement.

II. Another area-dependent characteristic is prominent in the ITO/GIO/Au device, but due to different RS mechanism. The XPS depth profile realized in this device revealed a significant change between the pristine state and the electroformed state. This change was most noticeable in the In/Ga atomic stoichiometric relation in the bulk region near the ITO layer. It was found more indium in the electroformed state than the pristine state of the device. The simulation of the physical parameters according to the model of thermionic emission portrayed significantly decreased series resistance, parallel resistance and ideality factor of the diode, but no change of the barrier height as also verified when the Au contact was peeled-off in vacuum (Annex 2). This suggests that some doping in the bulk regions is occurring, being explained with the ionic movement of the indium from the GIO layer to the ITO during electroforming. The resistance change occurred in the device was irreversible (stayed with the same diode behaviour when applying other reverse bias voltage and even higher or lower voltages in the same polarization). This may indicate, that Joule heating plays an important role in increasing the ion mobility during electroforming: The low current in reverse polarity causes a much-reduced temperature increase when compared to the forward direction, thus limiting the ion mobility for reset.

In summary, this work demonstrated that is possible to study the resistive switching mechanisms through XPS depth-profiling analysis. The XPS spectra enabled the observation of changes due to ionic movement or when it's the case, the absence of changes in the oxidation states that excludes this type of mechanism.

4.2 Perspectives for the near future

The in-operando approach was only partially-successfully in this work. It was demonstrated the possibility to realize electrical characterization and change the resistance state of the device, in the vacuum chamber of the XPS. The XPS can execute high-resolution analysis of an element using a continuous mode. This mode opens the opportunity, for example, to perform set and reset cycles while studying the chemical properties of the interface from the top electrode. However, the interactions of the X-ray beam with the device state need to be carefully taken into account.

Further analysis on the ITO/GIO/Au can be realized to understand the temperature dependency and its influence in RS mechanism of the device. It is possibly that the ionic motion of the device is due to a Joule heating when increasing the electric field intensity. This study can be extremely important to know the behavior of the effective temperature of the bulk, to build 2^{nd} - order memristors equations explored in the neural study. [31]

Finally, it is absolutely relevant to study the RS mechanisms while comparing the pristine state to a high resistance state (HRS) using the same XPS depth profile and electrical analysis utilized in this thesis for the LRS. It is equally important to comprehend the reset process and the set process.

References

[1] S. Slesazeck and T. Mikolajick, “Nanoscale resistive switching memory devices: A review,” *Nanotechnology*, vol. 30, no. 35. IOP Publishing, 2019.

[2] J. S. Meena, S. M. Sze, U. Chand, and T. Y. Tseng, “Overview of emerging nonvolatile memory technologies,” *Nanoscale Res. Lett.*, vol. 9, no. 1, pp. 1–33, 2014.

[3] J. S. Lee, S. Lee, and T. W. Noh, “Resistive switching phenomena: A review of statistical physics approaches,” *Appl. Phys. Rev.*, vol. 2, no. 3, 2015.

[4] F. De Stefano, M. Houssa, J. A. Kittl, M. Jurczak, V. V. Afanas'Ev, and A. Stesmans, “Semiconducting-like filament formation in TiN/HfO 2/TiN resistive switching random access memories,” *Appl. Phys. Lett.*, vol. 100, no. 14, 2012.

[5] R. Waser, “Electrochemical and thermochemical memories,” *Tech. Dig. - Int. Electron Devices Meet. IEDM*, pp. 1–4, 2008.

[6] R. Waser, R. Dittmann, C. Staikov, and K. Szot, “Redox-based resistive switching memories nanoionic mechanisms, prospects, and challenges,” *Adv. Mater.*, vol. 21, no. 25–26, pp. 2632–2663, 2009.

[7] S. Bagdzevicius *et al.*, “Superposition of interface and volume type resistive switching in perovskite nanoionic devices,” *J. Mater. Chem. C*, vol. 7, no. 25, pp. 7580–7592, 2019.

[8] C. Baeumer *et al.*, “Spectroscopic elucidation of ionic motion processes in tunnel oxide-based memristive devices,” *Faraday Discuss.*, vol. 213, no. 0, pp. 215–230, 2019.

[9] A. Sawa, “Resistive switching in rapid advances in information technology rely on high-speed and large-capacity nonvolatile memories,” *Mater. Today*, 2008.

[10] Y. Aoki *et al.*, “Bulk mixed ion electron conduction in amorphous gallium oxide causes memristive behaviour,” *Nat. Commun.*, vol. 5, pp. 1–9, 2014.

[11] M. Kot, “In-operando hard X-ray photoelectron spectroscopy study on the resistive switching physics of HfO2-based RRAM,” (PhD thesis, Brandenburg University of Technology Cottbus - Senftenberg, Bradenburg, Germany), 2014.

[12] A. Einstein, “Über einen die Erzeugung und Verwandlung des Lichtes betreffenden heuristischen Gesichtspunkt,” Annalen der Physik, vol. 322, no. 6, pp. 132–148, 1905.

[13] C. Weiland, A. K. Rumaiz, P. Pianetta, and J. C. Woicik, “Recent applications of hard x-ray photoelectron spectroscopy,” *J. Vac. Sci. Technol. A Vacuum, Surfaces, Film.*, vol. 34, no. 3, p. 030801, 2016.

[14] A. Klein, T. Mayer, A. Thissen, and W. Jägermann, “Photoelectron Spectroscopy in Materials Science and Physical Chemistry :,” *Bunsen-Magazin*, vol. 10, no. 4, pp. 124–139, 2008.

[15] Andrade J.D. (1985) X-ray Photoelectron Spectroscopy (XPS). In: Andrade J.D. (eds) Surface and Interfacial Aspects of Biomedical Polymers. Springer, Boston, MA.

[16] S. P. Kowalczyk, F. R. McFeely, L. Ley, V. T. Gritsyna, and D. A. Shirley, “The electronic structure of SrTiO3 and some simple related oxides (MgO, Al2O3, SrO, TiO2),” *Solid State Commun.*, vol. 23, no. 3, pp. 161–169, 1977.

[17] S. Tougaard, “Background removal in x-ray photoelectron spectroscopy: Relative importance of intrinsic and extrinsic processes,” *Phys. Rev. B*, vol. 34, no. 10, pp. 6779–6783, 1986.

[18] M. C. Biesinger, B. P. Payne, L. W. M. Lau, A. Gerson, and R. S. C. Smart, “X-ray

photoelectron spectroscopic chemical state Quantification of mixed nickel metal, oxide and hydroxide systems," *Surf. Interface Anal.*, vol. 41, no. 4, pp. 324–332, 2009.

[19] J. F. Moulder, W. F. Stickle, P. E. Sobol, and K. D. Bomben, "Handbook of XPS.pdf." p. 255, 1995.

[20] D. H. Kwon *et al.*, "Atomic structure of conducting nanofilaments in TiO2 resistive switching memory," *Nat. Nanotechnol.*, vol. 5, no. 2, pp. 148–153, 2010.

[21] D. Walczyk *et al.*, "Resistive switching behavior in TiN/HfO2/Ti/TiN devices," *IEEE 2012 Int. Semicond. Conf. Dresden-Grenoble, ISCDG 2012*, no. May 2014, pp. 143–146, 2012.

[22] T. Bertaud *et al.*, "In-operando and non-destructive analysis of the resistive switching in the Ti/HfO2/TiN-based system by hard x-ray photoelectron spectroscopy," *Appl. Phys. Lett.*, vol. 101, no. 14, pp. 1–6, 2012.

[23] C. Baeumer *et al.*, "Verification of redox-processes as switching and retention failure mechanisms in Nb:SrTiO 3 /metal devices," *Nanoscale*, vol. 8, no. 29, pp. 13967–13975, 2016.

[24] S. Brivio, J. Frascaroli, and M. H. Lee, *Electrical AFM for the Analysis of Resistive Switching*. Springer International Publishing, 2019.

[25] N. Branca, "Memristor based on amorphous zinc-tin oxide Schottky diodes," (Master's thesis, Universidade Nova de Lisboa, Lisbon, Portugal) , 2019. Retrieved from http://hdl.handle.net/10362/75825.

[26] H. Ji *et al.*, "Improvement in Field-Effect Mobility of Indium Zinc Oxide Transistor by Titanium Metal Reaction Method," *IEEE Trans. Electron Devices*, vol. 62, no. 4, pp. 1195–1199, 2015.

[27] T. Schultz, S. Vogt, P. Schlupp, H. Von Wenckstern, N. Koch, and M. Grundmann, "Influence of Oxygen Deficiency on the Rectifying Behavior of Transparent-Semiconducting-Oxide-Metal Interfaces," *Phys. Rev. Appl.*, vol. 9, no. 6, p. 64001, 2018.

[28] C. La Torre *et al.*, "Volatile HRS asymmetry and subloops in resistive switching oxides," *Nanoscale*, vol. 9, no. 38, pp. 14414–14422, 2017.

[29] S. L. Wang, C. Y. Chen, M. K. Hsieh, W. C. Lee, A. H. Kung, and L. H. Peng, "In-Ga-O based double-heater phase change memory cell," *2008 Jt. Non-Volatile Semicond. Mem. Work. Int. Conf. Mem. Technol. Des. Proceedings, NVSMW/ICMTD*, vol. 00, no. c, pp. 33–36, 2008.

[30] J. H. Werner, "Schottky barrier and pn-junction I/V plots - Small signal evaluation," *Appl. Phys. A Solids Surfaces*, vol. 47, no. 3, pp. 291–300, 1988.

[31] S. Kim, C. Du, P. Sheridan, W. Ma, S. Choi, and W. D. Lu, "Experimental Demonstration of a Second-Order Memristor and Its Ability to Biorealistically Implement Synaptic Plasticity," *Nano Lett.*, vol. 15, no. 3, pp. 2203–2211, Mar. 2015.

[32] C. J. Lee, Y. C. Chang, L. W. Wang, and Y. H. Wang, "Nonvolatile resistive switching memory utilizing cobalt embedded in gelatin," *Materials (Basel).*, vol. 11, no. 1, 2017.

[33] J. Shang *et al.*, "Highly flexible resistive switching memory based on amorphous-nanocrystalline hafnium oxide films," *Nanoscale*, vol. 9, no. 21, pp. 7037–7046, 2017.

[34] P. Schlupp, H. von Wenckstern, and M. Grundmann, "Schottky barrier diodes based on room temperature fabricated amorphous zinc tin oxide thin films," *Phys. Status Solidi Appl. Mater. Sci.*, vol. 214, no. 10, 2017.

Annex

Annex 1

It was also fabricated a shadow mask for the insulator layer and used in ITO/ZTO/Pt device. The design of this mask is shown in Figure 0.1.

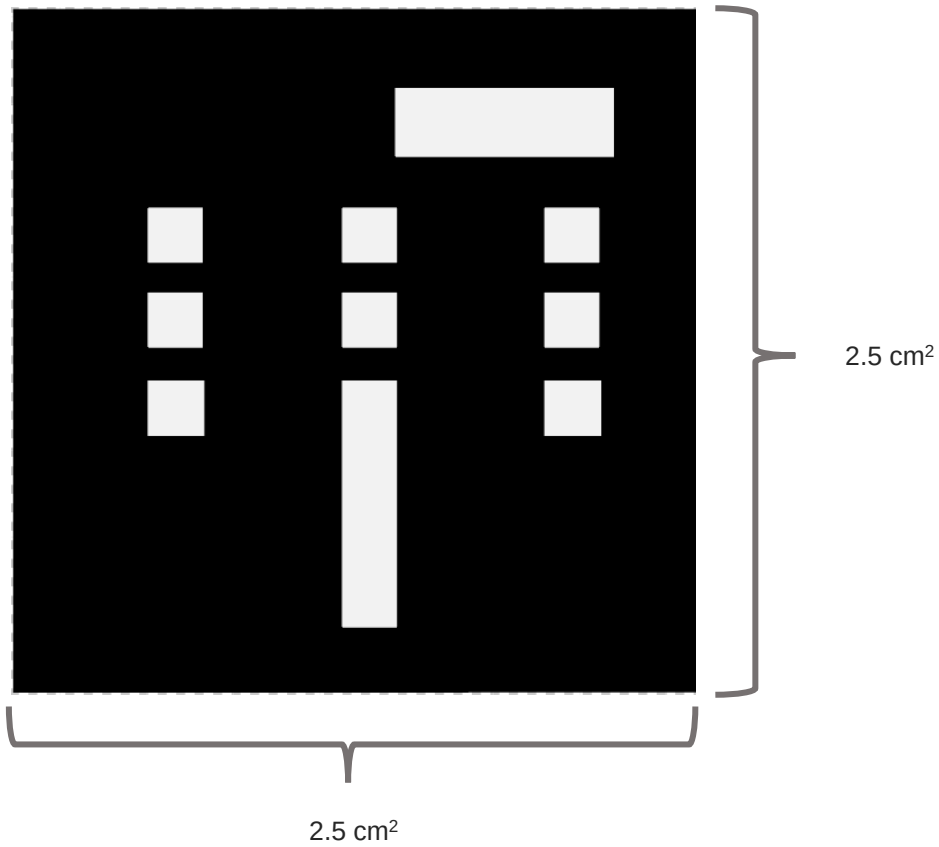

Figure 0.1 Shadow mask design that patterned the ZTO layer in ITO/ZTO/Pt.

The shadow mask wasn't used in the fabrication of the other devices due to shadow effects that occurred in the sputtering depositions creating unevenness in the insulator area. These different area sizes could be the reason for different pristine behaviours of the ITO/ZTO/Pt I-V characterization.

Annex 2

The depth-profile technique is a destructive technique, and sometimes can influence the results, so to dismiss an eventual error, an experimental “peel-off” was realized in the ITO/GIO/Au. This “peel-off” consisted in removing the TE layer with a Kapton tape, inside of the XPS Flexi-lock that is in vacuum.

This will allow to see the chemical impact on the top interface of the device when etching the gold layer with the argon sputtering.

In Figure 0.2 and Figure 0.3 are represented the component fittings used to chemically analyse the surface of the device when “peel-off”. Figure 0.2 and Figure 0.3 (a) represent the components fittings when in the pristine state, and Figure 0.2 and Figure 0.3 (b) in the diode state, of the Ga2p and In 3d, respectively.

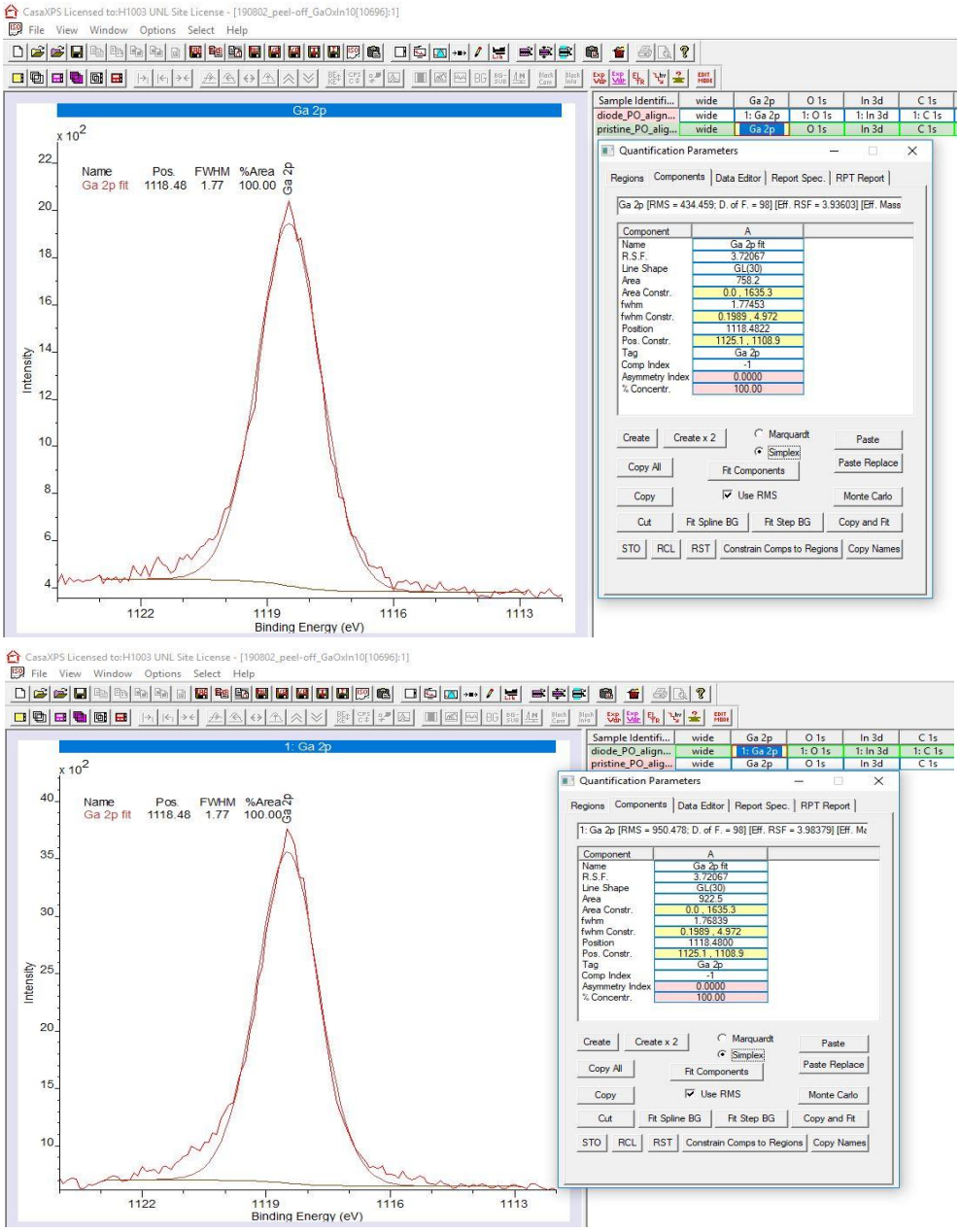

Figure 0.2 Ga 2p Fitting and components parameters for the peel-off of both (a) Pristine state and (b) Diode rectifier behaviour.

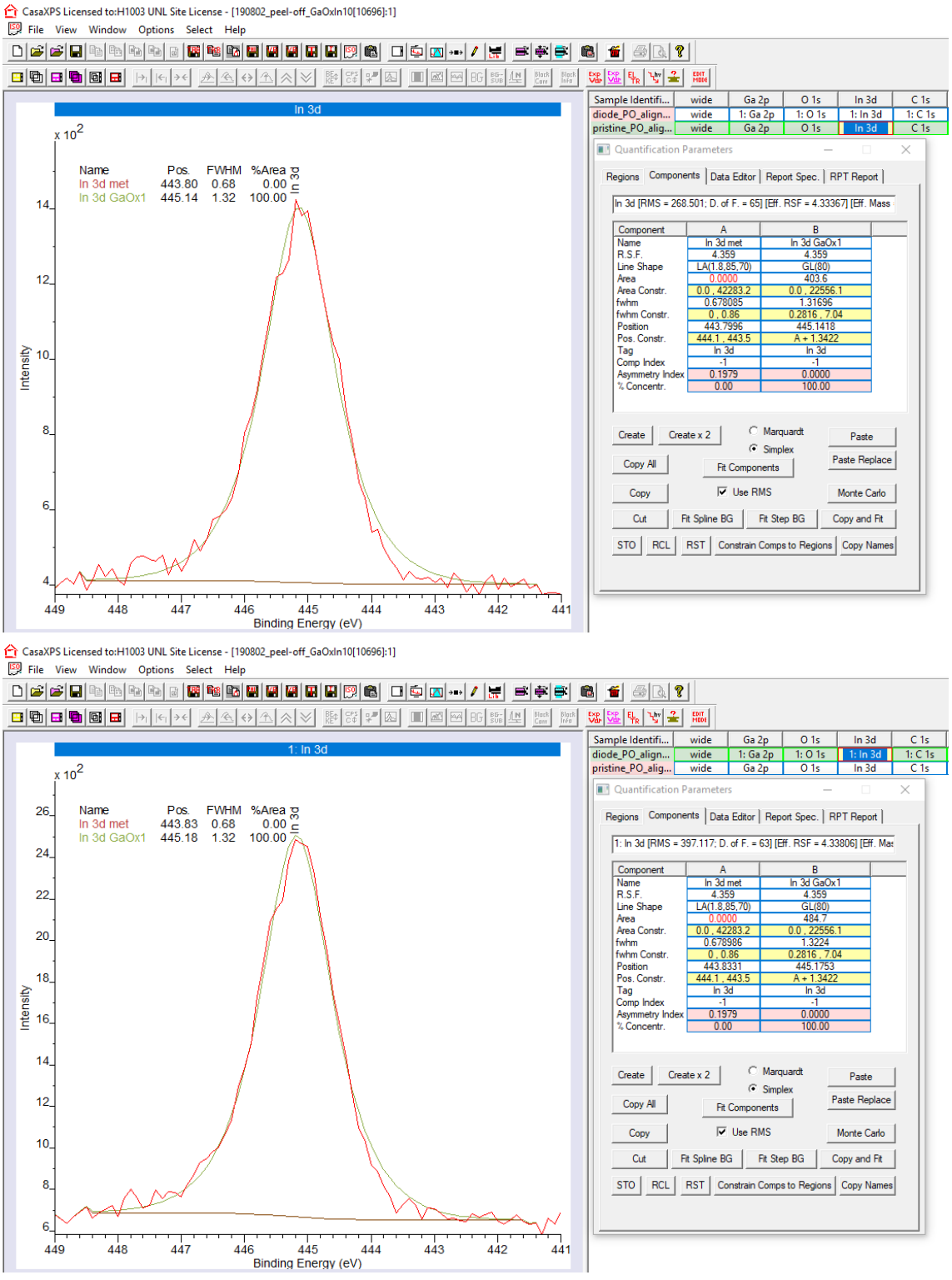

Figure 0.3 In 3d Fitting and components parameters for the peel-off of both (a) Pristine state and (b) Diode rectifier behaviour.

Figure 0.2 and Figure 0.3 are also representative of how the surface XPS software characterization was done for each etch time of every depth profile realized in this work.

After realizing this software analysis, we can extract the atomic percentages and calculate the difference between the Indium to Gallium and the metal to oxide component of indium, in this interface. The results are shown in Table 0.1.

Table 0.1 Atomic ratios of In/Ga and In metal / In oxide on the TE interface after the "peel-off".

	In/Ga	In metal/ In oxide
Pristine State	0.33	0
Diode State	0.32	0

These results show that similarly to the depth profile devices the In/Ga is nearly unchanged when comparing both states. An explanation for this is the barrier height maintaining also the same. In this aspect, the "peel-off" showed the same result as the depth profile. One big difference was that the "peel-off" device didn't show any metal component of indium, being this element totally oxidized when the surface was characterized.

Annex 3 ´

3.1 Analysis of Platinum as Top Electrode

The first sample fabricated had a BE composed by ITO, a widely utilized material as a resistive switching electrode, as can be shown in literature [32],[33]. The next two layers of both samples, ZTO and Pt, were deposited on top, where a Schottky barrier is formed. [34] The intention to put the Schottky barrier as top electrode was to allow an in-operando approach by XPS analysis by thinning the top electrode with argon cluster etching down to a platinum thickness low enough to capture a signal from the ZTO. Unfortunately, because of some problems that will be shown on sub-chapter three, and because of the electrical unevenness of the sub-devices of these samples compromised the XPS characterization.

3.1.1 Electrical characterization of ITO/ZTO/Pt

The first step of the electrical measure was to obtain an I-V (Current – Voltage) graph of the device right after the deposition of all layers. These I-V characteristics are named Pristine State, and are used to compare the differences after some electrical tests (SET, RESET, etc.) to the original electrical behaviour of the device. Table 5.2 lists the parameters of the electrical measurements to get the pristine information of the devices of ITO/ZTO/Pt.

Table 0.2 Parameters of Pristine I-V characterization of ITO/ZTO/Pt sample.

Parameters of Pristine I-V Characterization :	**Voltage dual sweep from** −1.5 V **to** 1.5 V
	Step: 0.01 V
	Number of Points: 602
	Compliance: 0.1 A

Two important aspects needed for the resistive switching analysis inside the XPS is that the pristine state of the nine devices of the fabricated sample are very similar between them, and simultaneously showing a high diode rectification ratio in the interface side. The study of the uniformity of the pristine state of the sub-devices are presented in Figure 0.4, having used the electrical parameters showed in Table 5.2.

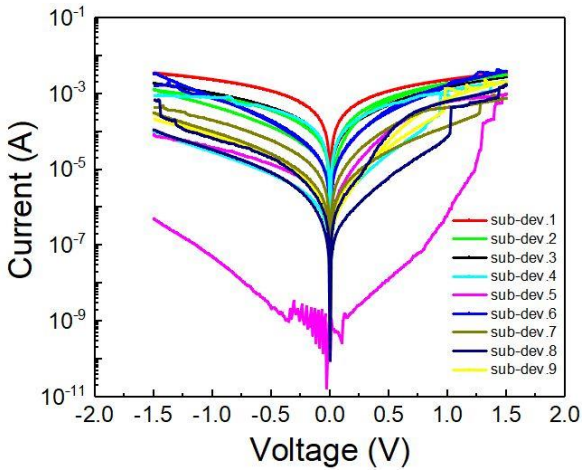

Figure 0.4 I-V characteristic comparison of pristine state of the nine sub-devices of ITO/ZTO/Pt sample.

It is clearly visible an unevenness in the pristine state between the devices of the sample, this may be due to a thickness oscillation in the layers throughout the deposited area of the samples. For example, a sub-device that is located closer to the evaporation target during deposition will theoretically be slightly thicker than a sub-device located farther way of the target. This factor alone it is not significant, but when combined to an undesirable shadow effect of the ZTO mask shown in Figure 0.1 of Annex 1 near the overlapping area of the electrodes, can induce this electrical discrepancy in the pristine states of the sample. The shadow effect is caused by approaching the resolution limit of aluminium plate shadow masks of about 500 µm.

Although no uniformity and good rectification was observed in this sample, an XPS measure was attempted just to modify the pristine state to a Low Resistive State (LRS) or to a High Resistive State (HRS) inside the main chamber. It chose the sub-device 8 with the pristine state exhibited in Figure 0.5, because it had the best rectification ratio without being too resistive (like the sub-device 7) or being too conductive (example of sub-device 1).

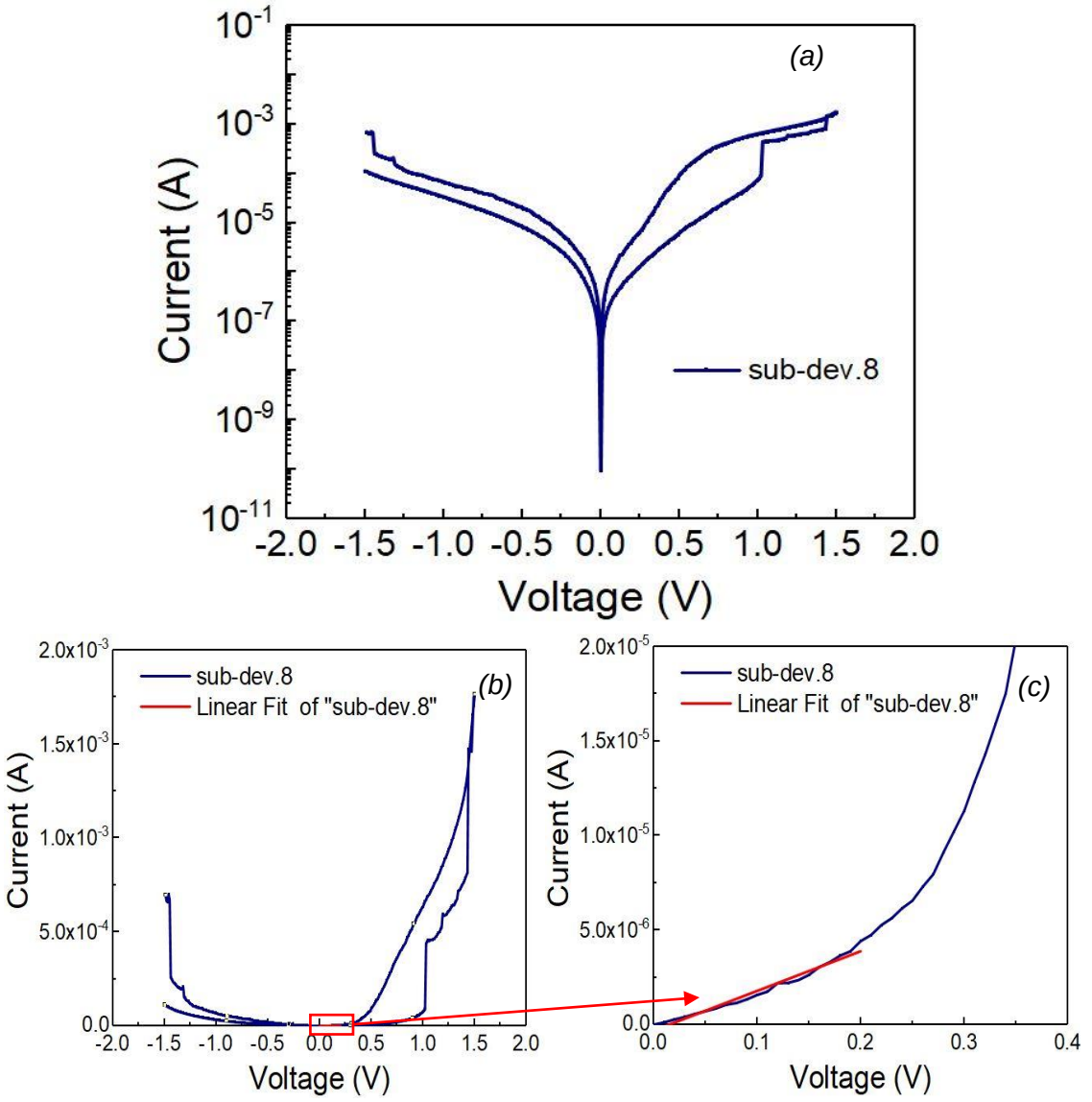

Figure 0.5 I-V characteristic of pristine state of sub-device 8 of ITO/ZTO/Pt sample. (a) logarithmic scale of current and (b) linear scale of current (c) linear regression fit from 0 to 0.2 V.

Before introducing the sample inside the XPS, it was carefully mounted in the holder and measured the resistance between the contact of the top electrode and the contact of the back electrode, with a multimeter applying about 0.2 V. The resistance value fluctuated between:

210-220 kΩ

To verify if the pristine state made sense in a practical perspective, a linear fit from 0 V to 0.2 V, represented in Figure 0.5 (b), was realized to know the resistance value of the sub-device 8.

After confirming that the value of the resistance of the I-V pristine graphs is in accordance with the values of the multimeter, the next procedure was to realize the electrical measure inside the XPS. Unfortunately, the first try wasn't well succeeded, after the introduction of the sample in the main chamber, it was measured again the resistance and the multimeter showed a short-circuit.

Annex 4

When the device was initiated with the in-operando approach it was possible to observe that it didn't lose all of the hysteresis when compared to the pristine state. So it was made another depth-profile to a device that portrayed a very similar hysteresis as the one showed in Figure 3.8 (f).

The atomic ratios represented in Figure 3.14 have different concentration of indium (the same 20% for pristine as used in the others GIO layers and 30% for the device with rectifier behaviour) but were calculated following the procedure described in the previous section.

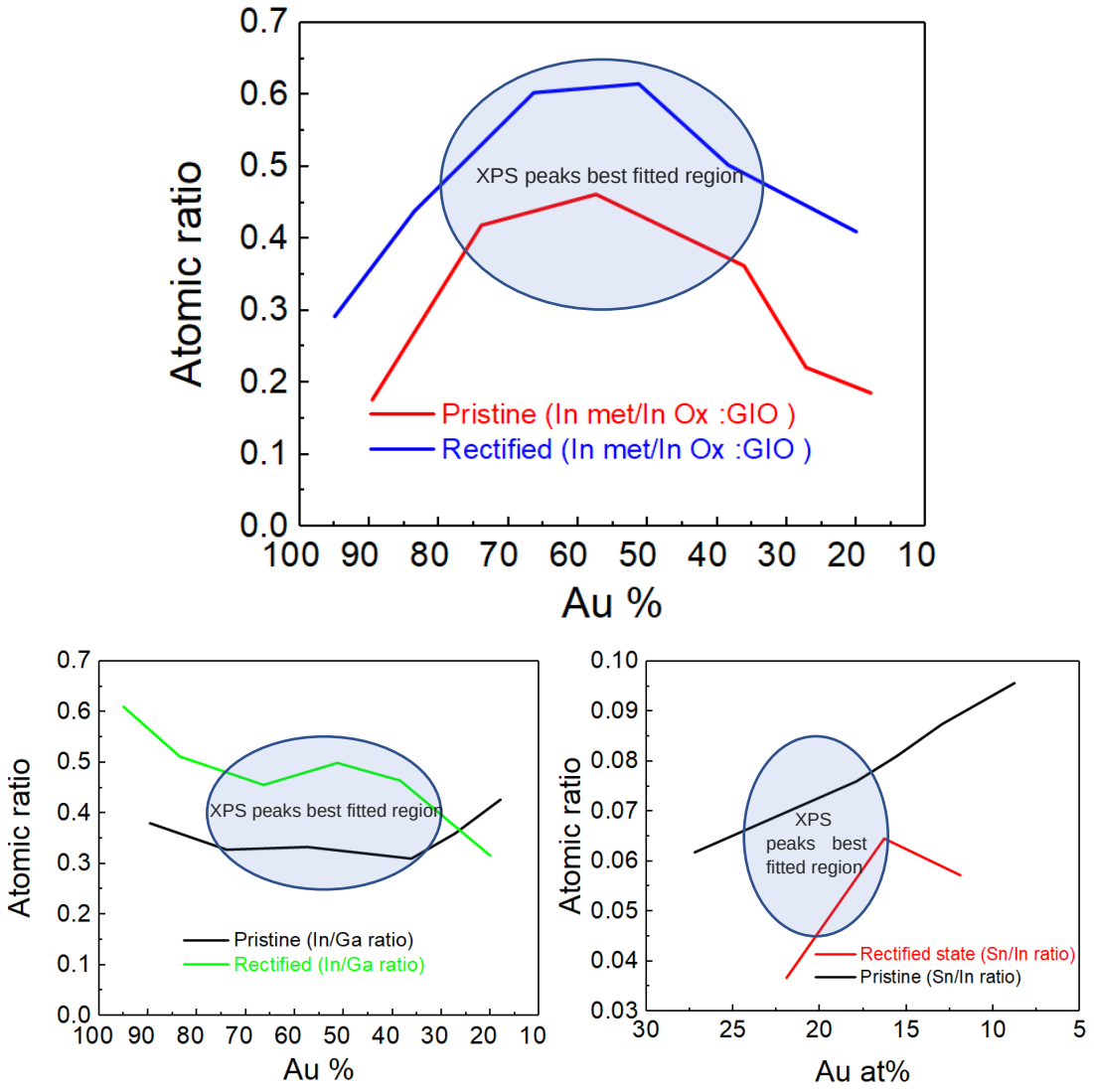

Figure 0.6 Analysis of a depth profiling of a device that shows no hysteresis after 8V.(a) Atomic ratio of metal components to oxide components of indium and (b) the atomic ratio of Indium to Gallium present in the GIO layer, in both diode and pristine state, in function of gold atomic percentage. (c) Atomic ratio of tin to indium, in the pristine and diode state, also in function of gold atomic percentage.

A bigger difference in indium to gallium is portrayed in Figure 3.14 (b) and (c) than the in-operando device displayed in Figure 3.13 (b) and (c), this was already expected since exists a 10% stoichiometric difference In:Ga deposition when deposited the GIO layer, from the pristine device to the electroformed device. It is interesting to see that the

behaviour of the ratios is identical in both cases giving veracity and reproducibility to these depth profile analysis.